THE ASTROPHYSICAL JOURNAL, 333:567–585, 1988 October 15

INTERACTING BINARY GALAXIES. V. NGC 4782/4783 (3C 278): UNBOUND COLLIDERS, NOT A SUPERMASSIVE PAIR

KIRK D. BORNE[1]
Space Telescope Science Institute;[2] and Department of Terrestrial Magnetism, Carnegie Institution of Washington
AND
MARC BALCELLS AND JOHN G. HOESSEL[1]
Washburn Observatory, University of Wisconsin, Madison
Received 1987 February 19; accepted 1988 March 31

ABSTRACT

The elliptical galaxies NGC 4782 and 4783 form a close pair with a very high relative velocity (658 km s^{-1} along the line of sight). This is indicative of either a very large system mass, a chance superposition, or an unbound encounter. From both the large relative velocity of the pair and the large central stellar velocity dispersions (392 km s^{-1} in NGC 4782; 297 km s^{-1} in NGC 4783), it would appear that one or both of these galaxies is very massive. Photometric distortions in the galaxies, whose shape and orientation are indicative of an intense tidal interaction, argue against superposition and in favor of a high-velocity encounter. In order to test these various hypotheses and to assist in the search for a viable interaction model for this system, CCD imaging data have been analyzed in conjunction with published spectroscopic measurements of this system. These data provide the input to our gravitational interaction model. Quantitative comparisons between the models and the data are made by using measurable indices that quantify the distortions seen in the galaxies. Strong constraints are imposed by the large relative velocity of the pair and by the degree to which the galaxies overlap. An excellent match between model and observation has resulted, permitting us to deproject the pair, to deduce the binary orbital parameters, and to determine the total system mass with a systematic error significantly smaller than that of standard mass estimators. Our best-fit model indicates that the binary orbit was hyperbolic before the encounter, but that energy loss during the collision has led to a loosely bound system. The pair will merge in 800 million years unless its binary orbit is disturbed by another member of the group of galaxies to which NGC 4782/4783 belongs. The total system mass in the region occupied by the luminous matter is found to be $1.4 \times 10^{12}\ M_\odot$ ($H_0 = 60$ km s^{-1} Mpc^{-1}), corresponding to a ratio of mass to blue luminosity of 10 (solar units). We are now observing the system just after closest approach, at an angle of $\sim 25°$ from the orbital plane. Our simulations confirm earlier theoretical studies which found that the internal velocity dispersions of colliding galaxies tend to increase just past closest approach, which then explains the large values measured for the central stellar velocity dispersions in these galaxies.

Subject headings: galaxies: clustering — galaxies: individual (NGC 4782/4783)

I. INTRODUCTION

This paper is one in a series of studies of isolated pairs of interacting galaxies (Borne 1984, 1988*a*, *b*; Borne and Hoessel 1988). A number of fundamental problems in extragalactic research are related to galaxy interactions (see White 1982 for a review): galaxy formation and evolution, cluster evolution, galaxy mergers, cD galaxy formation, star-formation activity, and nuclear activity. Binary galaxies provide a unique arena for the study of galaxy interactions since, lacking the complexity of systems that have a large number of galaxies, their dynamics are well defined, allowing detailed dynamical models to be constructed. Binary galaxy investigations are particularly suited to the study of the galaxy merger process.

Galaxy mergers can be understood as a straightforward consequence of dynamical and tidal friction, wherein the heating of the internal stellar distributions consumes external orbital energy. While some details may still be missing, it is clear that mergers must occur with exceedingly high frequency, as indicated by the number of systems with very distorted shapes (Arp 1966; Arp and Madore 1987), with bridges and tails (Toomre and Toomre 1972), and with shells (Malin and Carter 1983; Quinn 1984). The overabundance of multiple nuclei in first-ranked cluster galaxies (Hoessel and Schneider 1985) argues for ongoing merger processes even at the high-velocity dispersion cores of rich clusters (see Cowie and Hu [1986] and Tonry [1985] for two alternative views). Besides their intrinsic importance, merging galaxies provide interesting laboratories in which to test our understanding of the physics of gravitational interactions.

In this series of papers we address the merger problem in elliptical galaxies by numerically simulating the observed properties of binary systems and studying the effects of tidal friction on their orbits. Our study involves pairs with distinctly separate components and is thus complementary to studies of systems in an advanced state of merger where coalescence is nearly or totally complete, like NGC 7252 (Schweizer 1982; Borne and Richstone 1982, 1988), NGC 4838/39 (Quinn 1982), and shell systems (Hernquist and Quinn 1987). Since the binary systems that we are studying portray the initial, coher-

[1] Visiting Astronomer, Kitt Peak National Observatory, National Optical Astronomy Observatories, operated by the Association of Universities for Research in Astronomy, Inc., under contract with the National Science Foundation.

[2] Operated by the Association of Universities for Research in Astronomy, Inc., for the National Aeronautics and Space Administration.

ent reaction of the mass distributions to the tidal force, which is more easily modeled than the long-term evolution of an advanced merger product, our investigations permit the effects of tidal friction to be studied in detail.

Numerical simulations are run with the multiple three-body algorithm (hereafter MTBA), developed by one of us (Borne 1984, hereafter Paper I; Borne 1988*a*, hereafter Paper II), which has been used by Borne and Richstone (1988) to model NGC 7252, and by Borne and Hoessel (1988, Paper III) and Borne (1988*b*, hereafter Paper IV) for the analysis of the pairs K99 and K564 (Karachenstsev 1972). MTBA was also used in the dynamical study of the brightest galaxy in the cluster Abell 2052 (Kriss, Malumuth, and Borne 1988). While using a fixed potential approximation for the individual galaxies, the algorithm accurately accounts for dynamical and tidal friction, and its low computing cost makes it an efficient tool for a comprehensive search of model parameter space. The main products of the best-fit simulations are the parameters of the relative orbit, its three-dimensional orientation with respect to the observer, the energy and angular momentum change during the interaction, and a measure of the dynamical mass of the system that is free from the usual uncertainties of observer projection effects.

The pair NGC 4782/4783 (Fig. 1, Plate 17) bears special interest. The large relative velocity of this system was first reported by Page (1952) and subsequently by Greenstein (1961), whose values were used by Jenner (1974) in his dynamical study of supermassive galaxies. We work here with the redshifts and central velocity dispersions (Table 1) reported by Tonry and Davis (1981); their redshifts are very similar to those published earlier. In Table 1, our systemic redshift is corrected for the motion of the Local Group, but excludes the correction for infall toward Virgo. The high relative velocity (658 km s^{-1}) would suggest that this is not a physical pair but rather a chance superposition. Both components, however, show an obvious photometric distortion, indicative of physical association and, in particular, of a strong tidal interaction. The degree of distortion is demonstrated in Figure 2 (Plate 18) where we have turned up the contrast on the CCD image that was shown in Figure 1. We have whitened the pixels at which the two galaxies reach their peak surface brightness. Notice that the global brightness distribution is not symmetric with respect to the line connecting the brightness peaks. We will demonstrate that this marked asymmetry in the light distribution is an indication that a strong tidal encounter has just taken place. In § II we discuss and rule out the possibility that the observed pair is just a chance superposition of two unperturbed galaxies.

Both the high relative velocity of the pair and the high values of the central velocity dispersion in each galaxy (Table 1) suggest that at least one of these galaxies is extraordinarily massive. This is indicated by the relation between galaxy luminosity and velocity dispersion (Faber and Jackson 1976; Terlevich *et al.* 1981; Davies *et al.* 1983) (assuming also that the luminosity correlates with the mass of the galaxies). The central velocity dispersions are in fact unusual in that they are noticeably different, even though the two galaxies do not differ much in size and luminosity. Excessive galaxy masses are also indicated by the high relative orbital velocity in that the latter is so large that it suggests an observer line-of-sight nearly in the orbital plane, roughly parallel to the direction of the galaxies' motions. What is relevant and surprising about this conclusion is that from such a viewing angle most of the photometric distortion caused by the tidal interaction would not be observable (since the tides are symmetric with respect to the orbital plane), and yet the images of the galaxies are strongly asymmetric. Accordingly, the observer's line of sight must be far from the orbital plane, which would then require that projection factors significantly greater than unity be applied to any orbital mass estimate (see § III).

Another hypothesis that may explain the large velocities and the strong distortions that we measure in NGC 4782/4783 is one that assumes that a very close and fast passage is now taking place, with severe interpenetration of the two galaxies. A superposition of starlight and/or a tidal shock at closest approach may be the cause of the enhanced and distinctly different stellar velocity dispersions. An encounter on an initially unbound trajectory would then explain the high-relative velocity (without invoking large galaxian masses), and the photometric distortions would simply be the gravitational disturbances excited by the close encounter of the two galaxies.

We show in this paper that the high-speed close encounter hypothesis is similar to that which applies to galactic encounmore fully supported by all of the observations. An orbit solution will be presented, and it will be demonstrated that a gravitational shock is more than likely taking place, being responsible for the large internal velocity dispersions.

The dynamical configuration assumed in the fast encounter hypothesis is simiar to that which applies to galactic encounters in the cores of rich clusters. This investigation thus has relevance to the study of dynamical friction in the environments of cD galaxies (Hoessel, Borne, and Schneider 1985; Kriss, Malumuth, and Borne 1988).

This pair is also identified with 3C 278, an interesting radio source with twisted jets (L. Smarr, private communication). It would be of interest to relate the structure of the radio jets to the dynamical history that we are proposing for the system.

NGC 4782/4783 are the dominant members of a group of maybe 20–25 galaxies. De Souza and Quintana (1988) have given an estimate of the group's mass from measurements of radial velocities of the members and, assuming proportionality between mass and light, conclude that NGC 4782/4783 are supermassive. Their result does not contradict ours since we measure mass on a different scale length, but the existence of

TABLE 1

COORDINATES AND VELOCITIES FOR NGC 4782 AND 4783

Galaxy	R.A.[a]	Decl.[a]	V_r (km s^{-1})[b]	σ (km s^{-1})[b]	z systemic[c]
NGC 4782.....	12^h52^m0	12°18'.1	4608	392	0.0137
NGC 4783.....	12 52.0	12 17.4	3950	297	

[a] Equinox of 1950.
[b] Velocities from Tonry and Davis (1981), include Local Group correction.
[c] Luminosity-weighted redshift corrected for Local Group motion.

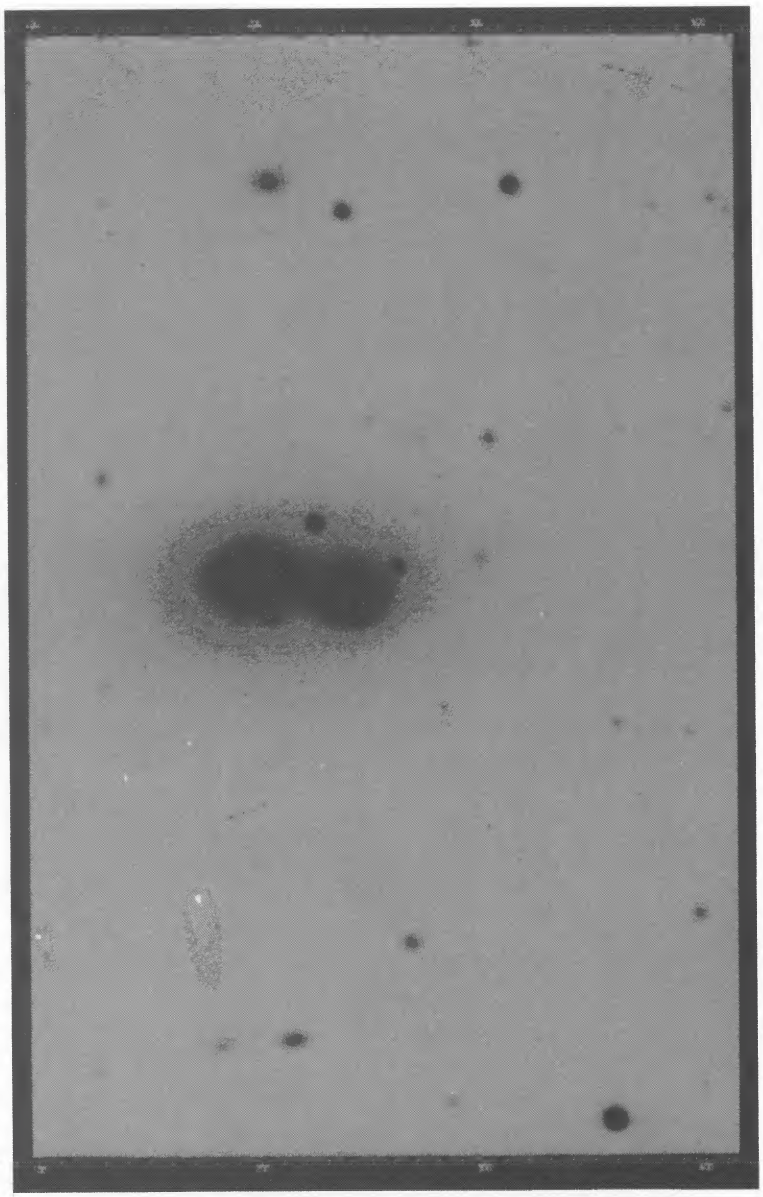

FIG. 1.—1200 s red CCD image of NGC 4782/4783. North is to the right, and east is down (reverse from the sky). The field is 4.'6 by 7.'3 (320 × 512 pixels). NGC 4782 (southern component) is the more luminous of the two galaxies. Several foreground stars are seen in projection quite close to the galaxies, and several small (presumably background) galaxies are also seen around the field.

PLATE 18

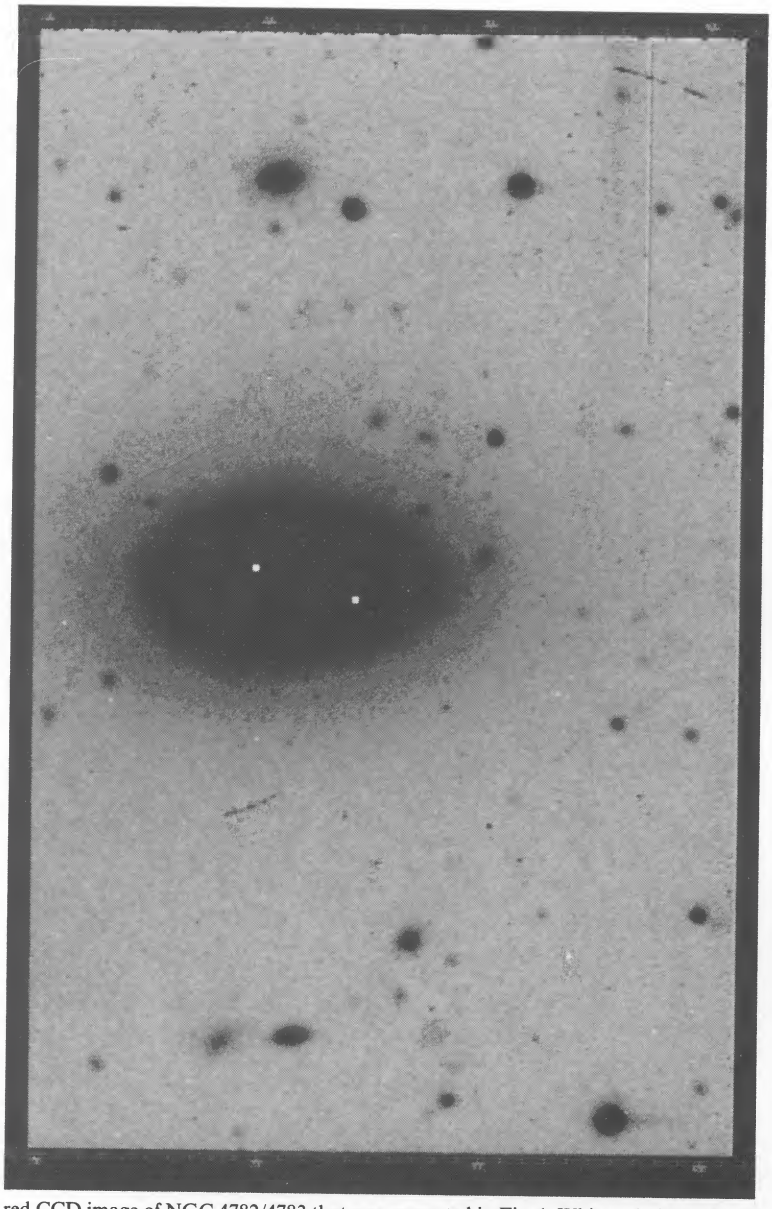

FIG. 2.—High-contrast copy of the red CCD image of NGC 4782/4783 that was presented in Fig. 1. Whitened pixels identify the brightness peaks (nuclei) in each of the two galaxies.

the group does call into question our treating the interaction as a binary problem. We will show that our approach is appropriate in this case, demonstrating that the binary interaction can be uncoupled from the group dynamics.

In the following sections we discuss new photometric observations of NGC 4782/4783 (§ II) and detailed numerical simulations of the system. Section IV describes our explorations of the available model parameter space. We compare the mass calculated from our best-match simulation to that obtained by application of various standard mass estimators (§ III and § V), and describe some of the physical processes at work during the interaction (§ VI). The group membership issue is addressed in § VII.

II. SURFACE PHOTOMETRY

a) *Observations*

Observations were carried out with the RCA no. 1 CCD at the R-C focus of the Kitt Peak 0.9 m telescope during the night of 1984 March 28–29. At f/7.5, the scale on the CCD was 0".86 pixel^{-1}. The night was photometric, as judged from frequent visual checks and from the residuals to the standard stars solutions ($\sim$1%), but seeing was poor, about 3".7 (FWHM). *B*, *V*, and *R* images were obtained, with exposures ranging from 400 s to 1200 s. Stars from the Landolt (1973) catalog were observed during the course of the night and used as photometric standards. Reduction of the raw CCD imaging data followed the standard procedure, including removing the bias, and flat-fielding using exposures of a uniformly illuminated target on the inside of the dome.

b) *Analysis*

The photometric analysis also followed the standard steps. Three small objects that appear projected against our galaxies were removed. Their pixel values were replaced with a bilinear interpolation of the border values. Neighboring star and galaxy images were similarly removed.

To measure the sky level in each passband, six circular zones were selected as far from the galaxies as possible. The mode of the pixel distribution was found in each zone and the six values were averaged. Standard deviations between the six values amounted to 1% in *V* and *B* and 0.5% in the *R* image. Magnitudes for each component of the pair were estimated by drawing a line across the narrowest portion of the overlapping contours to effectively split the pair into its two components. Magnitudes are given for each component and for the whole system in Table 2. Assigning a given line of sight to a particular galaxy is arbitrary since the galaxies are significantly superposed and stars dynamically bound to different galaxies are projected along the same line of sight. In addition, during the interaction a fraction of the stars in each galaxy ceases to be bound to either component. Still, we expect our magnitudes to provide a measure of the relative luminosity of the two components. This number is important for the dynamical study in the second part of this paper, as it provides an estimate of the binary mass ratio, as do the central velocity dispersions and the relative photometric sizes. To estimate the mass ratio from the ratio of luminosities one can either use the total magnitude of each object or else use the magnitudes measured out to the faintest surface brightness at which the two galaxies are still distinct, 20.0*V* mag arcsec^{-2} in our case. Neither of these options is particularly good. The first is affected by ambiguities arising from superposition and the somewhat arbitrary selection of the splitting line. The second provides, in principle, a better measure of the relative number of stars still bound to each galaxy, but does not account for material stripped during the interaction. For this pair, however, the two methods yield nearly identical results, $L_2/L_1 = 0.72$ and 0.68, respectively. The agreement in L_2/L_1 found by the two methods may indicate that the galaxies have been similarly stripped and that our line of sight views debris spread similarly across both members of the pair. The fraction of the total system light enclosed within the 20.0*V* mag arcsec^{-2} isophote is 0.23 for NGC 4782 and 0.16 for NGC 4783.

TABLE 2

MAGNITUDES AND COLORS

Galaxy	V^a	V^b	$B-V^c$	$V-R^c$	$B_{tot}{}^d$
NGC 4782.....	11.35	12.34	1.02	0.88	11.82
NGC 4783.....	11.68	12.76	0.98	0.86	

[a] *V* magnitudes, integrated down to $\mu_V = 25.0$ mag arcsec^{-2}.
[b] *V* magnitudes, integrated down to the critical isophote (faintest isophote at which the galaxies still appear distinct: $\mu_V = 20.0$ mag arcsec^{-2}.
[c] Colors, integrated to $\mu_V = 22.0$ mag arcsec^{-2}.
[d] *B* magnitude for the whole system, integrated down to the $\mu_V = 25.0$ mag arcsec^{-2}, assuming no galactic extinction.

Given the photometric distortions in NGC 4782/4783, it makes little sense to extract from our images the typical azimuthally averaged surface brightness profiles. Profiles for finite sectors around each galaxy are more interesting since they provide a quantitative measure of the isophote distortions and display effects such as tidal truncation and distension. We have therefore measured the radial brightness variations in two wedges originating at the center of each galaxy, both about 70° wide, one opening to the east and one to the west, the directions in which the maximum isophote compression and distension occur. Figure 5*a* shows the east and west profiles for NGC 4782 and Figure 5*b* the corresponding profiles for NGC 4783. The tidal pertubations are indeed severe, affecting the light profiles down to the very cores of the galaxies: 2 kpc for NGC 4782 and 1.6 kpc for NGC 4783 (marginally above the seeing). These distances are smaller than the effective radii of the four profiles (7.8 kpc and 18.3 kpc for the truncated and distended sides of NGC 4782, and 5.2 kpc and 12.6 kpc for the truncated and distended sides of NGC 4783). These effective radii, obtained by fitting de Vaucouleurs functions, bear little meaning as half-light radii since the real profiles do not follow an $r^{1/4}$ law owing both to the tidal perturbations and to the fact that the two galaxies are partially superposed. Hence, we do not plot the de Vaucouleurs fits for each individual profile. Instead, we plot the light profiles for the two model galaxies shown in Figure 4 (see below), along the same sectors that were used in the real galaxies. The galaxies in Figure 4 are pure undisturbed model galaxies, whose flattened light distributions follow the $r^{1/4}$ law exactly. They are used here to test the superposition hypothesis for the NGC 4782/4783 pair. As we mention in § I, the large relative velocity of the pair could easily be explained by a line-of-sight coincidence, and it is therefore necessary that we test this hypothesis.

The superposition model (Fig. 4) was constructed using effective radii derived from azimuthally averaged light profiles for each galaxy from which we excluded the sector where the light is dominated by the other galaxy. We also used the observed luminosity ratio (0.7) and the observed eccentricities of the faintest isophotes at which the two galaxies are still

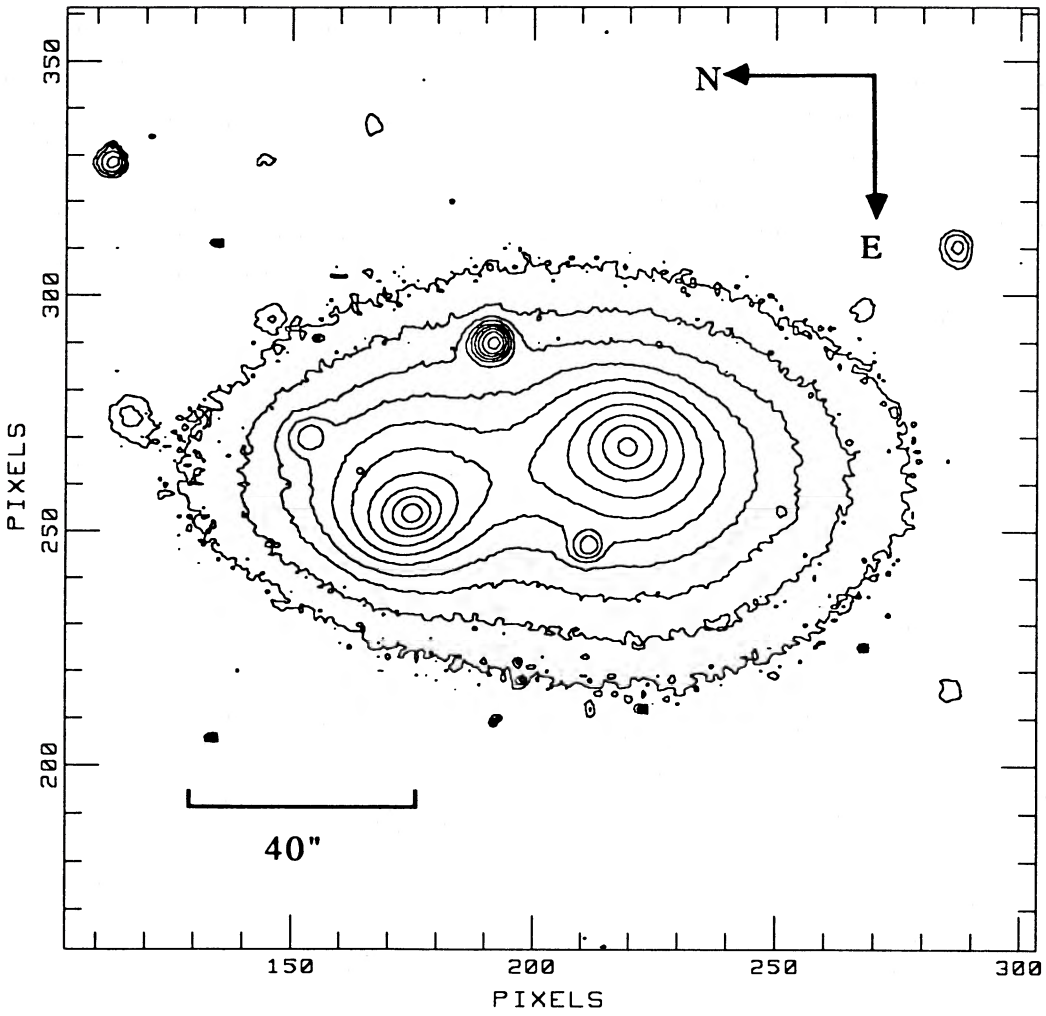

FIG. 3.—Surface brightness contour plot of NGC 4782/4783 from a 1200 s red exposure. Contours are every half-magnitude, starting at 18 R mag arcsec^{-2}.

disconnected. Several such models were constructed. The surface brightness profiles of the east and west sectors showed minimal asymmetry, with little sensitivity to reasonable changes in the model parameters. Since it is difficult to know *a priori* the values of the model parameters that would produce the best match to the data (e.g., superposition is likely to cause apparent rotation of the contours' major axes with respect to their true orientations in the isolated galaxies), we chose to base our analysis on a model with effective radii and eccentricities as described above but with major axes 20° from the projected separation vector, horizontal in Figure 3, in order to maximize superposition on the distended parts of each galaxy. This less realistic, best-case model is the one plotted in Figure 4. The profiles obtained from this model, plotted in Figures 5*a* and 5*b*, show the maximum possible asymmetry that can be obtained by superposition of these two unperturbed galaxies. In addition to the arbitrary major axis orientations, this model is also unrealistic because the effective radii of the model galaxies were obtained from fits to azimuthally averaged surface brightness profiles: if the distension/truncation in the galaxies were purely the result of superposition, then the individual true nonsuperposed surface brightness profiles would be better approximated by the profiles at the truncated sides of the superposed image, not by an average of both truncated and distended sides. Our use of an average effective radius, if anything, has maximized the already weak effect of superposition in our model and will thus strengthen the conclusion that the observed asymmetry is not the result of chance superposition of two unperturbed galaxies.

The differences between the two pairs of curves in Figures 5*a* and 5*b* are remarkable. The behavior of the real profiles is more pathological, especially in NGC 4783, the smaller member of the pair. Truncation is so severe that the superposition model profiles remain far above the real curves. The asymmetry also is strongest in the smaller galaxy. While in NGC 4782 both superposition model curves follow closely the distended observational profile, in NGC 4783 the observed profile from the distended side of the galaxy has an extended shoulder. Trying to increase the effective radius of the model galaxy to better fit the shoulder would make the galaxy's effective size too large compared with the real system and would make even worse the already lousy fit to the truncated side. The truncations and the shoulder are not a superposition feature and must be a signature of the interaction between the galaxies, which has caused intrinsic deformations in the galaxies' distribution of stars. Note that even though the synthetic

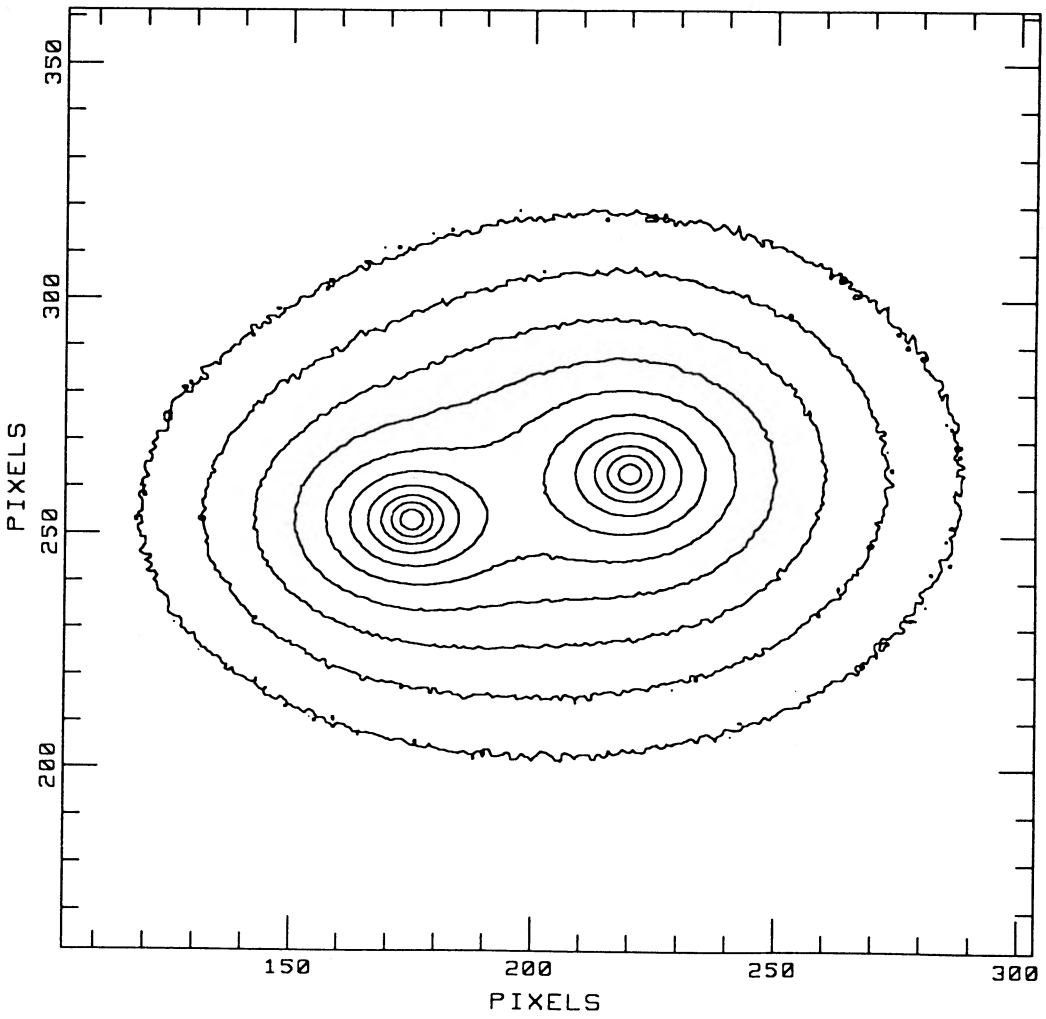

FIG. 4.—Superposition of two $r^{1/4}$ law galaxies, in an attempt to reproduce the contours in Fig. 3 by superposition of two unperturbed galaxies. Major axes have been oriented so as to maximize the contamination of the companion in the zones where the galaxies show the largest isophote distension.

profiles for the east and west sectors of each galaxy are not identical, due to contamination by the companion's light, the deviation occurs at much fainter brightness levels in the model galaxies than in the data. As expected, this divergence is strongest for the small galaxy. By comparison, the distended profiles for the real galaxies seem to be truncated at faint surface brightness levels. For both galaxies the profiles fall off more rapidly than the superposition of $r^{1/4}$ law model galaxies.

These qualitative differences make a case for the pair being a physical system rather than a line-of-sight coincidence, in spite of the large value of the relative radial velocity. We can actually demonstrate that it is impossible for any superposition of two symmetric elliptical galaxies to reproduce the brightness distribution seen in NGC 4782/4783. In the case of NGC 4782, at about 5 kpc radius, the east and west profiles differ by 0.75 mag arcsec^{-2}. If a superposition model were to create this contrast, NGC 4783 should be at least as bright as NGC 4782 in the area studied, or 21 mag arcsec^{-2}, in order to account for the factor 2 increase in brightness. This area is 40″ south of the center of NGC 4783 (see Fig. 3). At this same distance toward the north, NGC 4783 has a surface brightness of about 22.5 mag arcsec^{-2}. *Any* symmetric model will be deficient in the north by at least a factor of 4 in surface brightness to account for the profile distortion present in NGC 4782. A similar argument can be applied to NGC 4783. Thus, while the previous discussion brings up the point that some contour distortions *can* result from superposition, implying that caution must be taken when interpreting asymmetries as direct evidence for galaxy interaction, we find in the present case that each galaxy is too small, relative to the binary separation, to sufficiently affect the light profile of the companion by a superposition effect alone. Conclusively, NGC 4782/4783 is a physically associated system, and the observed contour crowding and distensions are the result of gravitational interaction between the members of the pair.

$B-V$ and $V-R$ colors were obtained from the CCD images. Mean values for each galaxy are given in Table 2. They are typical of elliptical galaxies showing no sign of star formation activity. A gradient in $B-V$ is present near the core of each galaxy, not unlike many normal elliptical galaxies (Fall 1981). The colors range from $B-V = 1.1$ at the centers to $B-V = 1.0$ at about 20″. At larger distances from the centers any preexisting color gradients would be diluted, both by superposition and by population mixing.

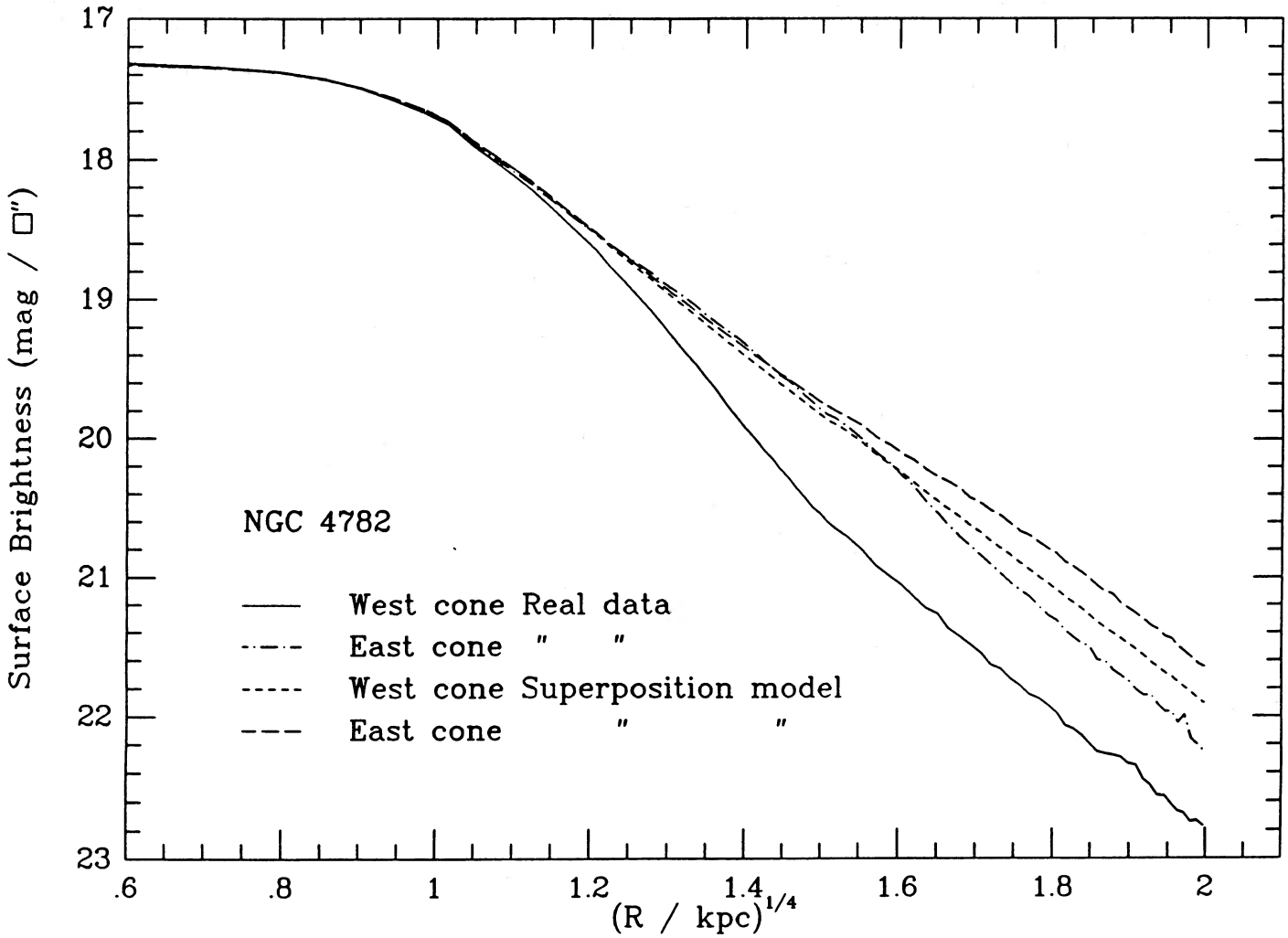

FIG. 5a

FIG. 5.—V surface-brightness profiles for (*a*) NGC 4782 and (*b*) NGC 4783, measured in 70° wide sectors oriented toward the west and east directions and originating at the center of each galaxy. Profiles for the real data and for the superposition model of Fig. 4 are displayed. The effect of superposition, if any, is to elevate the light profile above the straight line corresponding to the $r^{1/4}$ profile, whereas profiles for the real data appear truncated.

This pair of galaxies was studied 25 years ago by Greenstein (1962) and by Burbidge, Burbidge, and Crampin (1964). From scans along a line connecting the two nuclei, these investigators concluded that the smaller galaxy, NGC 4783, has a much lower central surface brightness than its companion. In fact, our higher signal-to-noise observations indicate that the small member is actually more centrally concentrated, as is the case in most normal ellipticals (Kormendy 1985).

III. PREDICTED MASS FROM STANDARD MASS ESTIMATORS

Since NGC 4782/4783 are physically associated, we must question whether their large relative velocity and the high central velocity dispersions are indicative of the very large masses that they appear to suggest.

A commonly used method for the determination of galaxy masses from observed velocities consists in calculating the potential energy from the observed density profile, estimating the kinetic energy from measurements of the internal velocity dispersion, and applying the virial theorem. Poveda (1958) applied this virial equilibrium method to an $r^{1/4}$-law model galaxy, and derived $M = 9\sigma^2 R_{\rm eff}/G$, where σ is the *global* one-dimensional dispersion and $R_{\rm eff}$ is the galaxy's effective radius. For our galaxies, we estimated $R_{\rm eff}$ from azimuthally averaged surface brightness profiles, yielding 17.7 kpc and 9.7 kpc for NGC 4782 and NGC 4783, respectively. Using the velocity dispersions quoted in Table 1, we obtained $\log M/M_\odot = 12.7$ for NGC 4782 and $\log M/M_\odot = 12.2$ for NGC 4783. The use of *central* velocity dispersions for σ may overestimate the derived masses by as much as a factor of 2 (Michard 1980; Bailey and MacDonald 1981). Our values are compared in Figure 9 (points labeled 4782′, 4783′) against the mass function of a random sample of elliptical galaxies compiled by Tonry and Davis (1981). All of the masses plotted here were calculated from Poveda's formula using central velocity dispersions. From this diagram we must conclude either that NGC 4782 is a very massive galaxy or that we have significantly overestimated it mass. Tonry (1983) and others have warned of large systematic errors that may be incurred when using Poveda's formula out of context, as, for instance, when the velocity dis-

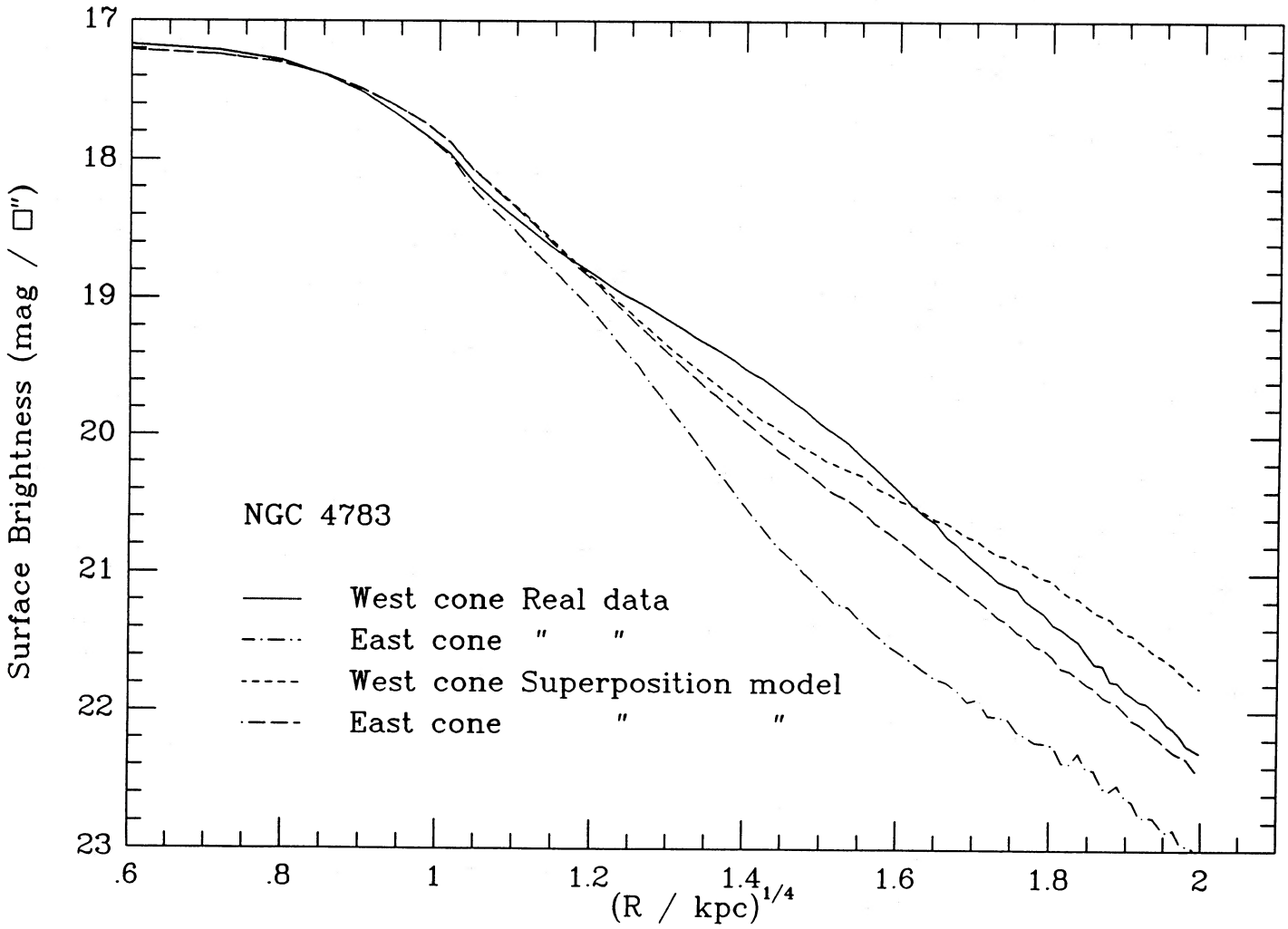

FIG. 5b

tributions are anisotropic. Major errors also appear if the galaxies are in fact not in dynamical equilibrium.

Another way to determine galaxy masses in close, isolated pairs is to assume that they form a bound binary. In this case a lower limit to the total mass of the system is given by $M_{\rm tot} > (\Delta v)^2 s/G$, where Δv is the line-of-sight relative velocity and s the projected separation. A statistically averaged value, accounting for the distribution of possible viewing angles, is about a factor of 3 above this lower limit, yielding $\log M_{\rm tot} \gg 12.1$ and $M/L_B \gg 13$. This estimate carries a large uncertainty due to our ignorance of the orientation of the orbit with respect to the plane of the sky, and assumes a binary separation of just 14.2 kpc, which implies that the galaxies significantly overlap one another.

The predicted mass for this pair is therefore quite high. The simulations described in the next section will in the end undermine the assumptions of virial and orbital equilibrium on which the above mass estimates depend.

IV. SIMULATIONS

a) The Algorithm

Simulations were run using a multiple three-body algorithm (MTBA, Papers I and II). The galaxies are modeled by a truncated isothermal sphere. The mass of the galaxies is distributed among N_1 and N_2 stars, with $N_1 + N_2 \leq 10{,}000$. In the MTBA approximation, the center of each galaxy feels the force given by the instantaneous distribution of stars in the companion galaxy, thus allowing for tidal and dynamical friction effects to operate. Each star, however, responds to the constant, though moving, spherical potentials of the unperturbed galaxies. This approximation neglects the self-gravity of the perturbations but has the advantage of being free of two-body relaxation. Computing time is strictly linear with N, making the algorithm efficient for comparison with observations, since fewer than 20 CPU minutes are required to compute a typical interaction from beginning to end on a Vax 11/780 machine using 1700 test particles. Merger times calculated with MTBA are slightly longer (by $\sim$50%) than times obtained using N-body integrators. This may be due both to MTBA having neglected the self-gravity of the galaxy's response to the perturbation (Miller and Smith 1980; White 1983) and to the N-body merger times being off because of unphysical transient torques (see Paper I) We shall show in § VI that the solution for NGC 4782/4783 obtained with an N-body code is very close to the MTBA solution. Only the internal dynamics cannot be totally reproduced with the fixed-potential model (i.e., the central velocity dispersions in the model cannot be made to match

those observed). The N-body reproduction of the MTBA orbit solution removes this deficiency.

A typical simulation run goes as follows. First, two galaxies of the desired masses, flattenings, and rotation are prepared, with numbers of stars proportional to their masses. The galaxies go through a mixing phase lasting typically five or 10 crossing times to erase traces of the initial configuration algorithm. After that, the galaxies are set in a relative orbit defined by the initial separation, velocity vector, and spatial orientation. Then the interaction starts. At prescribed moments during the interaction (typically every $\frac{1}{2}$ crossing time), we stop the evolution and observe the system from different viewing angles. Contour maps of the mass distribution, rotation curves, and velocity dispersion profiles are displayed, which can then be compared to observation. When a satisfactory match is found it means that we have determined the spatial orientation of the orbit in the sky, the velocity vectors, and the masses of the two components (in reduced model units, where $M_1 = G = R_1 = 1$; see Paper I). Physical units are regained by scaling the velocities and the projected separation to the observed values and the gravitation constant to its physical value (see § VIII). The process is necessarily interactive, given the large number of input parameters that need to be finely adjusted, and therefore a fast algorithm is essential. For the orbit search process discussed below, the interaction was simulated about 80 times.

b) *Parameter Space of the Simulations and Observational Constraints*

In the general formulation of the binary problem for elliptical galaxies there are 20 free parameters: mass ratio, luminosity ratio (or ratio of mass-to-light ratios), initial relative velocity and separation in the orbital plane (or, equivalently, initial speed and impact parameter at a given separation), spin vectors, galaxy flattenings, figure orientation, time of observation, and the direction of the observer. In the present case, however, since rotation curves have not been measured for either galaxy in the system, we have used nonrotating spherical galaxies. This reduces the parameter space to eight dimensions. Only in the final simulation did we add a reasonable amount of rotation and flattening.

Observational constraints imposed on any matching simulation include the ratios of central velocity dispersions to line-of-sight relative velocity, the ratio of luminosities, and the shape of the distortion seen in the system. A number of quantities can be defined for a shape comparison between the models and the real system. For the sake of consistency we have used as many as needed to obtain a total of eight observational constraints, to match the number of dimensions in our parameter space. Here we define the shape indices and describe their dependence on the physical parameters of the orbit. Interesting relations exist between subsets of the orbit parameters and the observational constraints: some constraints are helpful in determining the orbit orientation in the sky, while others probe the initial velocity and impact parameter, and so on.

The following shape indices have been defined:

$f_{\rm int}$ = ratio of masses (or luminosities, if M/L is constant) measured within the critical isophote (the faintest isophote at which the two galaxies still appear distinct).

$f_{\rm tot}$ = ratio of total masses (or luminosities) measured by splitting the system along a line perpendicular to the separation vector at the point of minimum surface density between the two galaxies.

χ_i = separation index: ratio of mass (or light) within the critical isophote in galaxy i to the total mass (or light) of the system.

β_i = compression angle: angle between the separation vector and the direction of greatest isophote compression, measured in the plane of the sky.

c_i = compression factor: ratio of radius of greatest compression to radius of maximum distension for galaxy i, measured at the contour 4 magnitudes below the central surface density.

(In the previous definitions and in the rest of this paper, ratios always refer to the ratio of the NGC 4783 value to the NGC 4782 value, and subscripts 1 and 2 refer to primary and secondary, that is NGC 4782 and NGC 4783, respectively).

The mass parameters $f_{\rm int}$ and $f_{\rm tot}$ are indicators of the relative sizes of the two galaxies. In our pair, $f_{\rm tot}$ is more affected by contamination than $f_{\rm int}$. Thus, a comparison between the relative values of $f_{\rm int}$ and $f_{\rm tot}$ in the models (mass ratios) and their relative values in the observations (flux ratios) places constraints on the mass-to-light ratios of the two galaxies (see more detailed discussion in § VII).

Separation indices χ_i and the ratios of central velocity dispersions to line-of-sight relative velocity are very sensitive to the angles between the line of sight and the separation vector and between the line of sight and the relative velocity vector, respectively (see Paper II). These indices thereby help to locate the angle of observation: at any given time the lines of sight where the model matches the observed ratios $\sigma_i/V_{\rm rel}$, if they exist, define a cone around the relative velocity vector; similarly, lines of sight that reproduce the observed values of χ_i define another cone, around the separation vector. In order to match the two parameters from the same observing angle it is necessary that the two cones of acceptable viewing angles intersect. This occurs either nowhere (no solution) or along two lines of sight, and it is always straightforward to choose between the two viewing angles from the resulting shape (i.e., parity) of the distortions in the system. Therefore, at a given time, the observing angles are determined by the separation indices and the velocity data (see detailed discussion in Paper II).

The compression angles β_i and the compression factors c_i are sensitive to the geometry and to the duration of the interaction, but they vary slowly with viewing angle. Thus these indices determine whether the initial velocity, impact parameter, and time of observation of the simulation are adequate. They are the main discriminators among different trajectories in the final tuning of the orbit solution. Initial speed and time of observation are also constrained to some extent by the ratios $\sigma_i/V_{\rm rel}$ and the separation indices χ_i. This is especially true for high-eccentricity orbits near closest approach when the velocity changes rapidly, as is the case with NGC 4782/4783.

The values of the observational constraints for the real system are shown in the first line of Table 4. The uncertainties in the compression angles β_i result in part from variations in the direction of maximum isophote compression with contour level. We do not assign errors to the other quantities since the uncertainties associated with their measurement in the observations is significantly smaller than in the simulations.

c) *The Orbit Solution*

To begin a search for the best matching simulation, one must decide on a value for the mass ratio. The observed luminosity ratio is a good starting point. Holmberg (1937) estimated photographic magnitudes for these galaxies. His ratio $L(4783)/$

L(4782) is 0.69, nearly identical to that estimated from our CCD images. Burbidge, Burbidge, and Crampin (1964) estimated the mass ratio for the system by assuming that the contact point for the brightest common isophote corresponds to the inner Lagrangian point of the binary system. They estimated the mass ratio to be 0.69, the same as Holmberg's luminosity ratio. Given the exact equality of these two values, we assume that NGC 4782 and 4783 have the same mass-to-light ratio, and that their mass ratio is 0.7 (see discussion at the end of § VII). For completeness, we ran test models with mass ratios $M_2/M_1 = 0.26$, 0.43, 0.70, 0.80, and 1. The first value corresponds to the one implied by the ratio of central velocity dispersions and the Faber-Jackson (1976) relation; this is probably not an acceptable value since these galaxies are far from dynamical equilibrium.

Experience in model-matching (Papers II and IV) provided a valuable help during the orbit search process. The strong asymmetries in the surface brightness contours imply a very strong interaction, especially since the high relative velocity suggests an observer line of sight not far above the orbital plane, where the asymmetries in the light distribution should be less conspicuous. As in Paper IV, we confirmed that the galaxies are moving in the direction of their compressed contours. Such a light distribution (i.e., opposing distensions for the two galaxies) is a sure indicator of the sense of binary motion in elliptical pairs that are so disturbed (Papers II and III).

We ran many trial simulations with different values for the initial speed and impact parameter. The search was a delicate one: distortions in the surface density were easy to produce simply by choosing an observing angle far enough from the orbital plane, but then the velocity data could not be matched (see Fig. 6). Conversely, when the velocity constraint was satisfied (i.e., with the correct σ_i/V_{rel}), the contour asymmetries would usually disappear behind the galaxies. A working combination of speed and impact parameter was ultimately found by trial and error. For this solution not only did the duration and intensity of the interaction produce the correct distortion at the time when the velocities were correct, but also the curvature of the orbit was such that the truncated and distended patterns visible in each galaxy were of the proper intensity and had the right orientation with respect to the separation vector. Our best simulation matched all of the observational constraints except for the ratio of central velocity dispersions. This was to be expected since the fixed-potential approximation in MTBA cannot account for the gravitational shock that is ultimately responsible for the observed dispersions. This problem is fully addressed in § VI*a*.

After a reasonably good solution was found, the parameter space around it was explored first to determine the best possible match and second to measure the range of acceptable solutions. Keeping the initial mass ratio at its value of 0.7 and working with initial separation of 4.0, only two parameters describe each run: initial speed and impact parameter. The impact parameter was increased/decreased in steps of 0.1, and at each value we ran simulations along the initial speed axis in increments of about 10% to search for a matching solution. Figure 7 displays, within the structure of that parameter space, contour plots of the corresponding systems at the times and observing angles that offered the best tentative matches. All the quantities relevant to this search are shown in Tables 3 and 4. Except when otherwise noted, all quantities are in reduced units (see § VIII for conversion to physical units). Orbits are listed in order of increasing impact parameter. The first column in each table contains the run number. When a given run number appears more than once, this means that two different

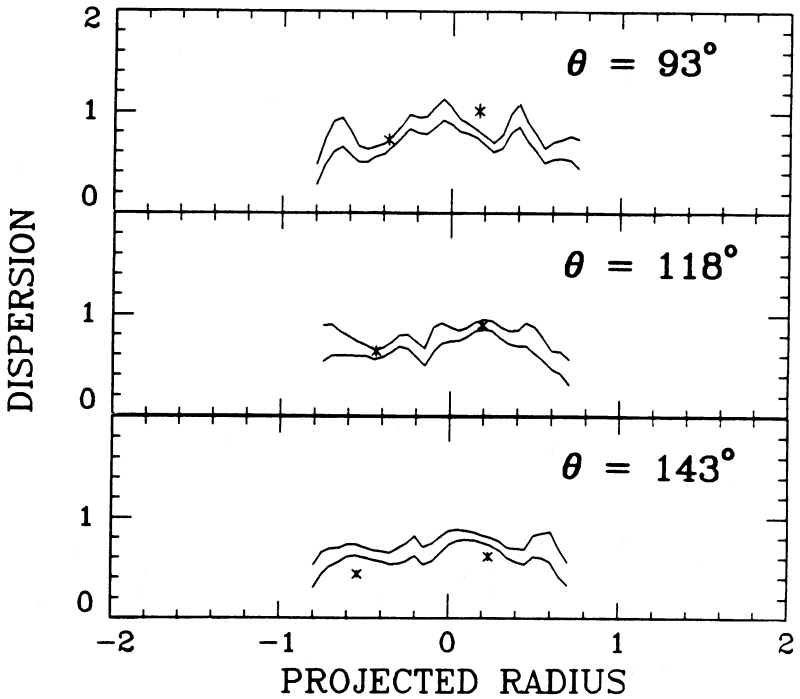

FIG. 6.—Line-of-sight stellar velocity dispersion profiles for an N-body simulation of NGC 4782/4783 (see § VI*a*). Scaled Tonry-Davis dispersions are represented by the asterisks and are scaled to units where the projected relative velocity of the real binary equals that of the model. Three observer viewing angles are presented here to demonstrate how changing the model observer's viewing angle affects the scaling and, hence, the match between model and observation.

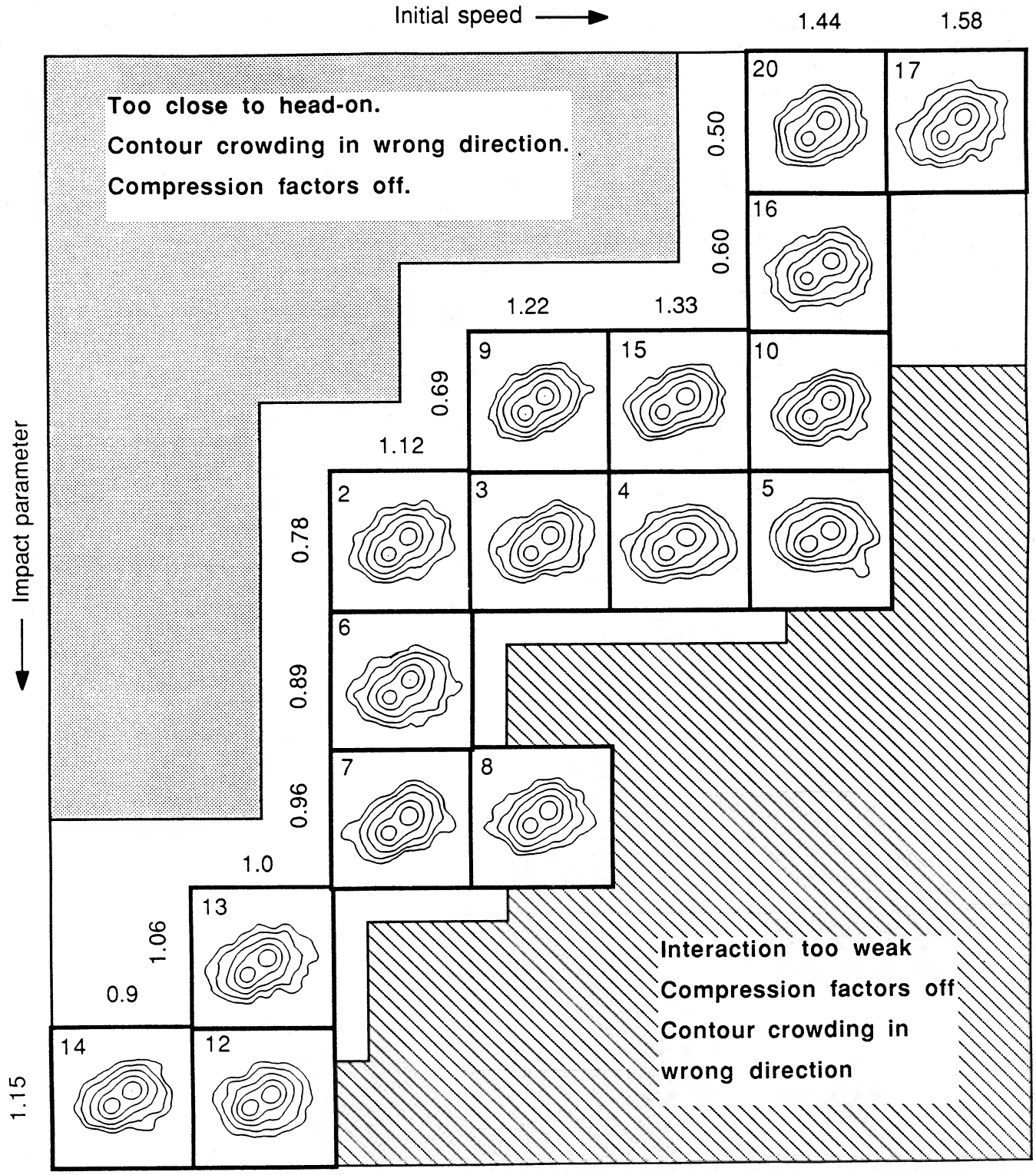

FIG. 7.—Surface density maps for simulations that were run in the final tuning of the orbit solution, represented in the initial velocity—impact parameter space. Mass ratio was 0.7 and initial separation was 4 in all cases. Each run is identified by its initial speed and impact parameter. Observing times and viewing angles have been chosen in each case so as to maximize its similarity to the real system (model parameters are listed in Table 3).

TABLE 3

ORBITAL DATA FOR MODEL SIMULATIONS

Run (1)	V initial (2)	Impact Parameter (3)	Time since Pericenter (4)	θ obs (deg) (5)	ϕ obs (deg) (6)	Separation (7)	Phase (deg) (8)	Speed (9)	Projected Separation (10)	Vel (LOS) (11)	k (12)
Real System ...	...	...	...	...	...	...	...	...	40″	658 km s^{-1}	...
20	1.46	0.5	0.39	65	−145	0.94	−153	1.89	0.45	1.70	...
19	1.50	0.5	0.44	65	−145	1.03	−159	1.90	0.49	1.71	...
18	1.54	0.5	0.47	65	−150	1.11	−157	1.86	0.48	1.64	1.30
17	1.58	0.5	0.52	65	−150	1.20	−157	1.85	0.52	1.63	1.22
16*	1.46	0.6	0.38	65	−140	1.12	−155	1.82	0.54	1.63	1.18
a16	1.46	0.6	0.38	65	−140	1.12	−155	1.82	0.55	1.63	1.17
9	1.22	0.7	...	65	−130	0.75	−162	2.03	0.48	1.84	...
15*	1.33	0.7	0.34	65	−130	0.79	−163	2.02	0.51	1.88	0.93
15*	1.33	0.7	0.44	65	−140	1.00	−155	...	0.49	1.63	1.31
a15	1.33	0.7	0.34	65	−137	0.79	−163	2.07	0.46	1.82	1.12
10	1.46	0.7	0.35	65	−140	0.85	−165	2.11	0.48	1.89	...
2	1.12	0.8	0.40	65	−130	0.88	−154	−1.82	0.49	1.64	...
3*	1.22	0.8	0.28	65	−130	0.71	−165	...	0.47	1.93	0.97
3*	1.22	0.8	0.40	65	−135	0.91	−155	1.87	0.48	1.66	1.29
a3	1.22	0.8	0.28	65	−130	0.71	−166	...	0.48	1.81	1.08
4	1.33	0.8	0.30	65	−140	0.74	−169	...	0.45	1.97	0.97
4	1.33	0.8	0.42	65	−145	0.95	−159	1.96	0.45	1.68	1.32
5	1.46	0.8	0.31	60	−155	0.80	−171	2.21	0.44	1.77	...
6	1.12	0.9	...	60	−135	0.81	−158	...	0.49	1.62	...
7*	1.12	1.0	0.31	65	−130	0.76	−162	2.02	0.49	1.81	1.06
a7	1.12	1.0	0.31	65	−130	0.79	−161	1.97	0.49	1.73	1.16
13*	1.00	1.1	0.32	65	−125	0.77	−157	1.92	0.49	1.71	1.19
a13	1.00	1.1	0.32	65	−125	0.77	−158	1.94	0.50	1.76	1.11
14	0.90	1.2	0.25	60	−125	0.64	−165	2.10	0.48	1.81	...
14	0.90	1.2	0.38	65	−120	0.82	−152	1.82	0.52	1.63	...
12	1.00	1.2	0.30	65	−135	0.72	−166	2.03	0.46	1.77	...
21	1.00	1.1	0.31	65	−120	0.69	−159	1.99	0.49	1.88	0.99

times gave an acceptable fit. As described below, an asterisk next to a run number identifies the run as a member of the family of best matches. Run numbers beginning with an "a" are also described below. In Table 3, columns (2)–(6) list physical characteristics of the orbits; taken together with the mass ratio, the initial separation, and the assumed unit ratio of mass-to-light ratios, these are the eight quantities that we wish to know about NGC 4782/4783. Columns (7)–(9) contain orbital data measured at the time of observation, while columns (10) and (11) list the quantities necessary to compute the mass of the system from observables (projected separation and line-of-sight relative velocity). The derived quantity k shown in column (12) is the mass projection factor that will be defined in § V. In Table 4, columns (2)–(9) present the observational constraints that are used to test the match of each model to the real system: mass ratios $f_{\rm tot}$ and $f_{\rm int}$, separation indices χ_i, compression angles β_i, and compression factors c_i. Note that the values in column (3) are derivable from columns (4) and (5) and so they do not provide independent information. Taken together with one of the ratios of velocity dispersion to relative velocity, these quantities provide the eight observational constraints used to isolate the orbit solution.

The systematic errors in the model measurements listed in Table 4 are difficult to estimate, our models being only poor representations of real galaxies. We have therefore set these criteria following repeated measurements of similar models: the separation indices χ_i are uncertain to 15%; the compression angles β_i are deemed acceptable if they lie within the range of uncertainty in the angles that were measured for the real system, as listed in row (1) in Table 4; and the compression factor c_i have a typical measurement error around 10%. We do not quote uncertainties for the mass ratios $f_{\rm int}$ and $f_{\rm tot}$ since these quantities are not really used as orbit discriminators but are used primarily to determine the observer viewing angle.

As described in § IV*b*, the main orbit discriminators are the angles β_i and compression factors c_i. Only at the outer limits of the explored domain in Figure 7 do we start to encounter problems in locating an observer orientation that matches both the velocity data and the separation indices χ_i. In the rest of the cases these can be matched arbitrarily well by simply fine-tuning the viewing angle. Therefore our strategy is to find that time and observing point where the velocity data and the ratios χ_i are in agreement with observation, and then to measure β_i and c_i, thereby determining the quality of the fit.

The orbits that were found to yield a reasonably good match were runs 16, 15, 3, 7, and 13. These models define a one-dimensional sequence in Figure 7, wherein an increase of impact parameter, accompanied by a decrease in the initial speed, brings the galaxies to similar degrees of interpenetration. As seen in Table 4, these orbits match two or three of the observational constraints. Runs 16, 15, 3, 7 and 13, marked with asterisks in the first column of Tables 3 and 4, have very similar pericenter distances, 0.35 ± 0.03, and they yield their best approximation to the data at very similar binary separation ($R = 0.80 \pm 0.07$), phase ($-159° \pm 4°$), and relative speed (1.96 ± 0.08), despite having initial conditions that cover a range of 33% in speed and 57% in impact parameter. Such initial configurations correspond to ranges of initial orbital

energy and angular momentum of $0.03 < E_0 < 0.19$ and $1.08 > L_0 > 0.92$, respectively. Each of these five runs was repeated using 10,000 particles, in an attempt to isolate the best possible model. These simulations are indicated in the first column of Tables 3 and 4 by an "a" preceding the run number. In practice, we found that increasing the signal-to-noise ratio in the models made them more similar to one another, and the overal fit to the data was slightly poorer than in the 1700 particle models. Run "a13" appeared to give the best match to the data, although its differences from the other "a" models are very small. Keplerian values (i.e., in the point-mass approximation) of the pericenter separation and speed for the inbound orbits of the best models are plotted in Figure 8. The upper curve in this figure corresponds to the locus of parabolic orbits and the lower curve to circular orbits. Our binary models are thus slightly hyperbolic. Paper II discusses the usefulness of this representation of parameter space in identifying the physical processes at work in interacting binaries. An analysis of this figure is presented in § VI.

For each of our five best orbits, the partial match to observation is lost for a 10% change in the initial speed. Compare, for instance, runs 9, 15, and 10 in Table 4. Note also that run 4, which is close to run 3 in Figure 7, provides a marginal match to the data (two parameters match) and thus yields a measure of the allowable range in initial velocity for a solution. Beyond this limit, for higher initial velocity, the trajectories are less penetrating and the interaction weakens; for smaller velocities, the interaction is stronger but the perturbations in the mass distributions do not have the right orientation and are not visible at the right time (Fig. 7).

TABLE 4

SHAPE PARAMETERS FOR MODEL MATCHING

Run (1)	f_{tot} (2)	f_{int} (3)	χ_1 (4)	χ_2 (5)	β_1 (deg) (6)	β_2 (deg) (7)	c_1 (8)	c_2 (9)
Real system ..	0.72	0.68	0.23	0.16	70 ± 5	65 ± 10	0.6	0.55
20	0.74	0.64	0.26	0.17	35	35	0.8	0.69
19	0.74	0.57	0.28	0.16	38	45	0.73	0.73
18	0.74	0.65	0.29	0.19	50	66	0.6	0.61
17	0.75	0.69	0.27	0.19	25	58	0.69	0.61
16*	0.75	0.68	0.28	0.19	82	62	0.64	0.74
a16	0.76	0.68	0.30	0.20	78	78	0.75	0.70
9	0.81	0.73	0.26	0.19	50	55	0.73	0.78
15*	0.78	0.74	0.26	0.19	68	68	0.76	0.68
15*	0.74	0.70	0.24	0.17	58	60	0.74	0.71
a15	0.77	0.69	0.24	0.16	69	60	0.62	0.71
10	0.76	0.66	0.29	0.19	75	40	0.67	0.70
2	0.78	0.74	0.24	0.18	55	60	0.78	0.70
3*	0.77	0.69	0.26	0.18	75	70	0.60	0.59
3*	0.77	0.74	0.24	0.18	75	70	0.63	0.57
a3	0.77	0.71	0.26	0.19	...	56	0.74	0.74
4	0.75	0.68	0.24	0.17	50	80	0.60	0.71
4	0.70	0.73	0.23	0.16	58	58	0.59	0.64
5	0.78	0.87	0.22	0.20	40	40	0.69	0.62
6	0.80	0.71	0.25	0.18	62	40	0.65	0.65
7*	0.77	0.66	0.26	0.17	75	85	0.67	0.71
a7	0.77	0.68	0.27	0.19	64	60	0.68	0.72
13*	0.81	0.76	0.24	0.18	40	75	0.64	0.59
a13	0.78	0.71	0.27	0.19	...	72	0.75	0.67
14	0.79	0.72	0.27	0.19	55	40	0.70	0.74
14	0.78	0.69	0.31	0.21	55	55	0.70	0.82
12	0.79	0.80	0.24	0.19	55	50	0.73	0.73
21	0.76	0.70	0.37	0.26	77	68	0.58	0.47

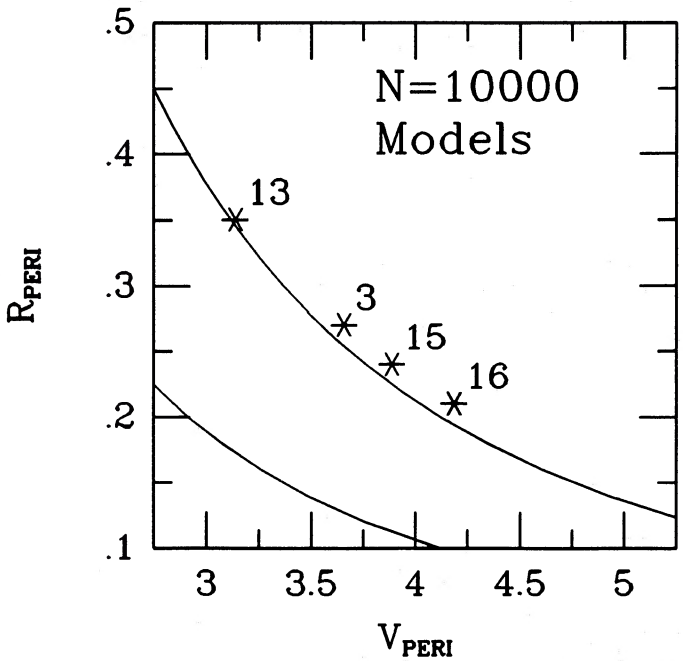

FIG. 8.—Parameters of the initial binary orbits for the best simulations that used a spherical nonrotating galaxy model. Each of these was run with $N_1 + N_2 = 10{,}000$ particles. Orbits are identified by their run number (models labeled "a" in Tables 3 and 4) and by their initial "Keplerian" pericenter speed V_{peri} and pericenter separation R_{peri}; simulations a7 and 21 are not plotted here since their initial orbits were nearly identical to that of model a13. Model units are converted to physical units in § VIII. The upper curve identifies the locus of parabolic trajectories, and the lower curve represents circular orbits. Binary trajectories situated above the upper curve are unbound, those in between the two curves are bound, and those below the lower curve are forbidden.

Orbits with impact parameter of 0.5 have nearly identical trajectories; pericenter distances are ~0.24, the deflection of the orbits is small, and we find it particularly difficult to locate a correct observing angle since the relative velocity and the separation vectors are nearly parallel. Tides exist but are not usually apparent from the relevant observing angles. Because the incoming speeds are high, we must let these systems separate significantly more than in the rest of the runs, which allowed us to match one or two of the observational constraints. However, the overall solution is essentially lost. We do not consider it necessary to explore smaller impact parameters since in this range of values the trajectories become more independent of the initial conditions. The solution is also lost at an impact parameter of 1.2 (runs 12, 14), where none of the model indices match their observational counterparts.

In many runs f_{tot} is higher than the observed value. This is a consequence of the galaxies' superposition and may mean that a slightly lower initial mass ratio (~0.65) would have been more appropriate.

We conclude that, for a given mass ratio, the acceptable orbit solutions lie in a single, limited, one-dimensional region of parameter space defined by models 13, 7, 3, 15, and 16. Beyond the limits of that region contour crowding is either too weak or has the wrong orientation with respect to the separation vector. Far enough from this region, matching both the velocity data and the mass-projection indices simultaneously becomes impossible, and the solution is completely lost. The

region of the solution is therefore unique, and it is unnecessary to explore regions of parameter space disconnected from it.

d) Internal Properties of the Galaxies

The solution found in the previous subsection is valid only within the context of its underlying model galaxy, i.e., spherical galaxies with no rotation. By adding flattening and rotation the match can be improved significantly. Even though we cannot constrain the internal dynamical parameters due to the lack of rotation curves and velocity dispersion profiles, we can provide an example of how our models may change with the addition of flattening and rotation. This example is identified as model 21 in Tables 3 and 4. Its initial orbital parameters are identical to those for run 13 (with $N_1 + N_2 = 10{,}000$), and the mass ratio is again 0.7, but now both galaxies are flattened like an E4 galaxy when seen along the orbital plane, and they each include a small amount of rotation. Rotation is added to the models by reflecting the sense of motion for 15% of the particles in each galaxy such that these will circulate in the same sense around the galaxy (prograde with respect to the orbit). This amount of rotation is typical of elliptical galaxies (Davies and Illingworth 1983). Although the fit did not improve for all of the parameters, it did for many of them, and this model provided the best overall visual similarity to the real system. A contour plot is shown in the insert to Figure 10. The small amount of rotation that was added has allowed the extensions to the north and to the south of the pair to grow to an extent similar to that of the real galaxies. This suggests that some rotation may indeed be present in these galaxies, which should be verified by long-slit spectroscopic observations.

We show in Figure 10 the orbital paths of NGC 4782 and 4783 on the plane of the sky, as determined from the simulation for model 21, where the tick marks indicate positions at 10^8 yr intervals, and the origin of the coordinate system is the binary center of mass. Such a map could find application in the analysis and interpretation of the twisted jets seen in radio images of this system, which is also known as 3C 278.

V. DYNAMICAL MASS OF THE PAIR

The knowledge of the three-dimensional orientation of the orbit in the sky allows an unambiguous calculation of the total dynamical mass of the pair. M_{tot} is given by

$$M_{tot} = k[\Delta v/(1+z)]^2 s/G \quad (1)$$

with

$$k \equiv (M_1 + M_2)/[(\Delta v)^2 R_{proj}] , \quad (2)$$

where quantities refer to the real galaxies in the first formula and to the simulated system in the second. Values of k for those simulations that match at least two of the control parameters have been listed in column (12) of Table 3. All the simulations yield very similar values of k, which means that the total mass of the system is very well constrained by the models. We obtain an average value of $k = 1.17$ with an uncertainty of less than

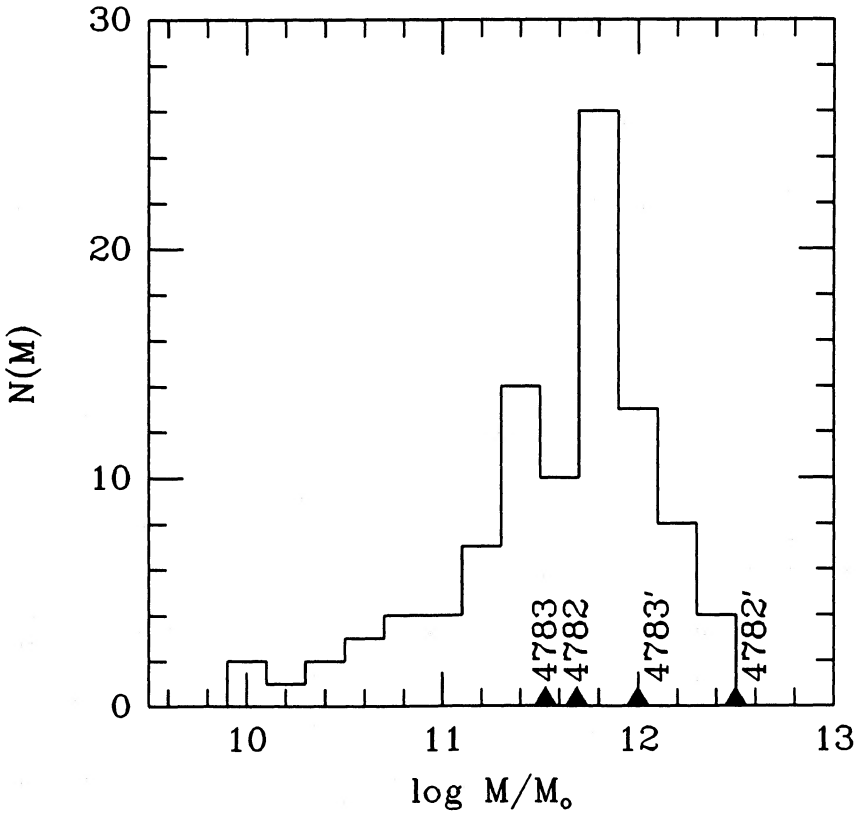

FIG. 9.—Histogram of dynamical masses for 98 ellipticals for which Tonry and Davis (1981) measured central stellar velocity dispersions. Dynamical equilibrium is assumed (see § III) in the calculation of the 98 masses represented in the distribution. The two symbols labeled 4782′ and 4783′ give the masses calculated for NGC 4782 and 4783 assuming that they too are in dynamical equilibrium. The two symbols labeled without primes give the masses derived for NGC 4782 and 4783 from our best-fit interaction model and orbit solution.

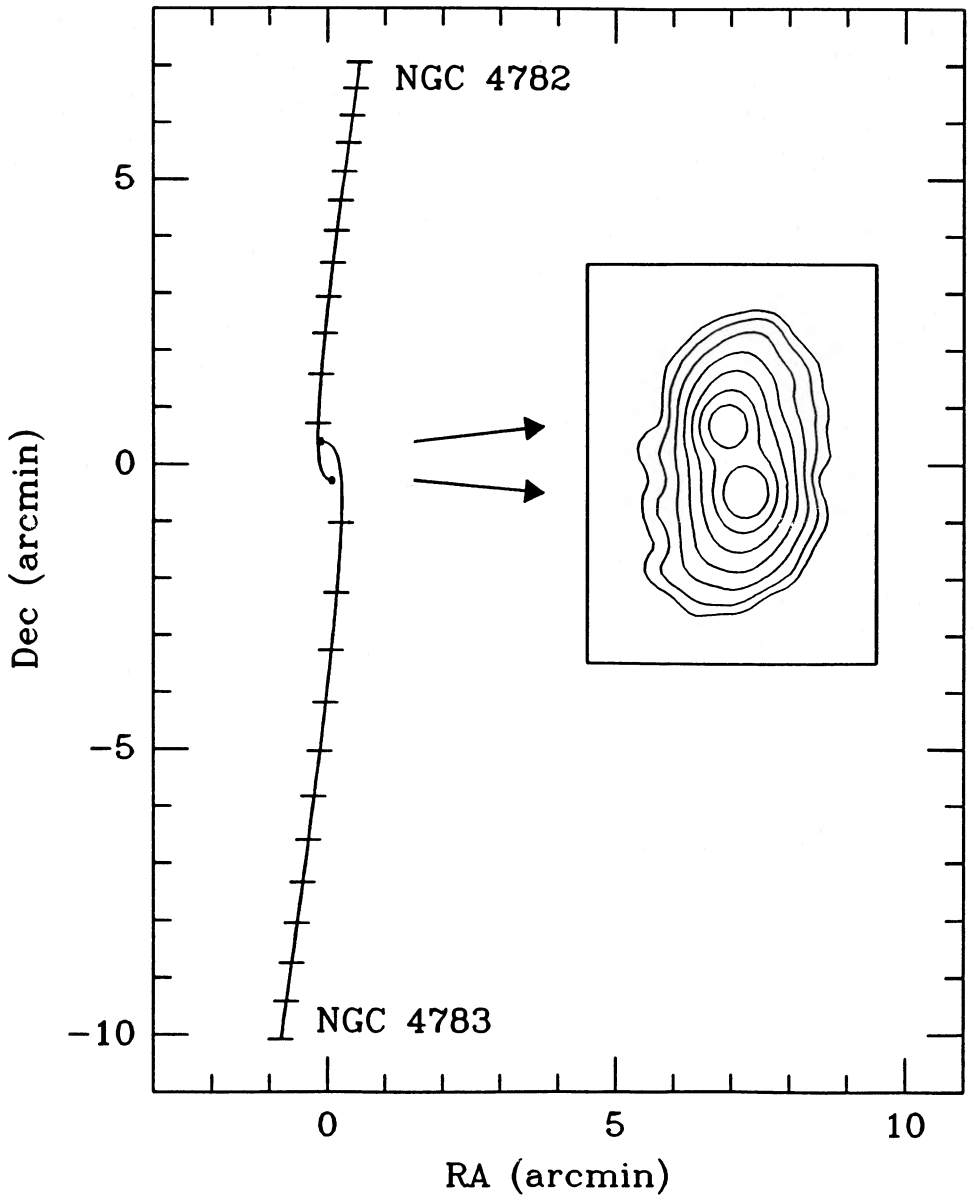

FIG. 10.—Trajectories for NGC 4782 and 4783 on the sky as derived from our best model (number 21 in Tables 3 and 4), and a surface density map for that simulation as seen from our deduced viewing angle. R.A. and Decl. are right ascension and declination offsets in arcmin from the system center of mass (i.e., luminosity-weighted center). The endpoints near (0, 0) indicate the current observed positions of these galaxies, and tick marks correspond to intervals of 10^8 yr.

30%, coming mainly from the ambiguity of the time of observation (see runs 3, 4, and 15). The masses of the galaxies are then $M(4782) = 8.1 \times 10^{11}\ M_\odot$ and $M(4783) = 5.6 \times 10^{11}\ M_\odot$, with an uncertainty of at most 30%, and the corresponding mass-to-blue luminosity ratio is 10. The location of these masses in Figure 9 is indicated by the points labeled "4782" and "4783" (unprimed symbols). Their location in the mass histogram indicates that NGC 4782 and 4783 are not supermassive but rather average-mass galaxies. Almost identical mass values are obtained from an N-body solution of the orbit (§ VI*a*).

VI. PHYSICAL PROCESSES

a) Tidal Shocks

As described in § IV, we have successfully derived a physical solution for the NGC 4782/4783 binary configuration. Our solution matches well most of the observable properties of the system except for the central velocity dispersions of the two galaxies. When faced with this failure to explain the large central velocity dispersions, we realized that MTBA was not equal to the task. The significant interpenetration of the galaxies at closest approach and the resultant tidal shock demand a self-consistent treatment of the stellar response to the strongly nonlinear disturbances within the galaxies (see discussion in Paper I and in Miller and Smith 1980). In order to model these disturbances correctly and to confirm the applicability of our orbit solution to the interpretation of the internal dynamics of the two galaxies, we ran a fully self-consistent N-body simulation with a code prepared by one of us (K. D. B.). The initial orbit of the pair in this calculation was identical to that for one of the $N = 10{,}000$ models described in § IV*c*. We used orbital parameters equaling those of model 3, with $N_1 = 1000$ par-

ticles and $N_2 = 700$ in the two model galaxies. The N-body simulation was run on a VAX 8800, consuming ~ 27 hr of CPU time in going from the initial binary configuration to the final merger product (corresponding to 12 units of model time). For comparison, this same model 3 was also evolved on the VAX 8800 using MTBA, with the same number of particles and for the same number of time steps, and this simulation required less than 4 minutes of CPU time to run. These two runs thus determined the scaling between the speed of our unpolished N-body code and the speed of the very efficient MTBA: MTBA is faster by a factor $N/4$, where N is the number of particles used in a simulation.

Figure 6 demonstrates that an N-body simulation can indeed produce the correct central velocity dispersions in the two galaxies. The middle box in that figure presents the model dispersion profile at the best viewing angle for the N-body model. The central stellar velocity dispersions indeed turn out to be anomalously high for the two model galaxies at the time of observation: in a small aperture around the nucleus, the line-of-sight velocity dispersion in each model galaxy is $\sim 30\%$ larger than it was at times prior to the close encounter. These enhancements are found to be significant when compared to the much smaller statistical fluctuations seen at other times (see Fig. 11 and discussion below), and they lead to a factor of ~ 3 overestimate of the masses when using the dynamical equilibrium equation (§ III). As demonstrated below, this reflects both the action of a tidal shock at the point of closest approach and the effects of light contamination from the other galaxy. Since these galaxies are not in dynamical equilibrium, any simple-minded derivations of their masses that are based on such an assumption, as in § III, will fail miserably. This conclusion lends support to the recommendations of Miller and

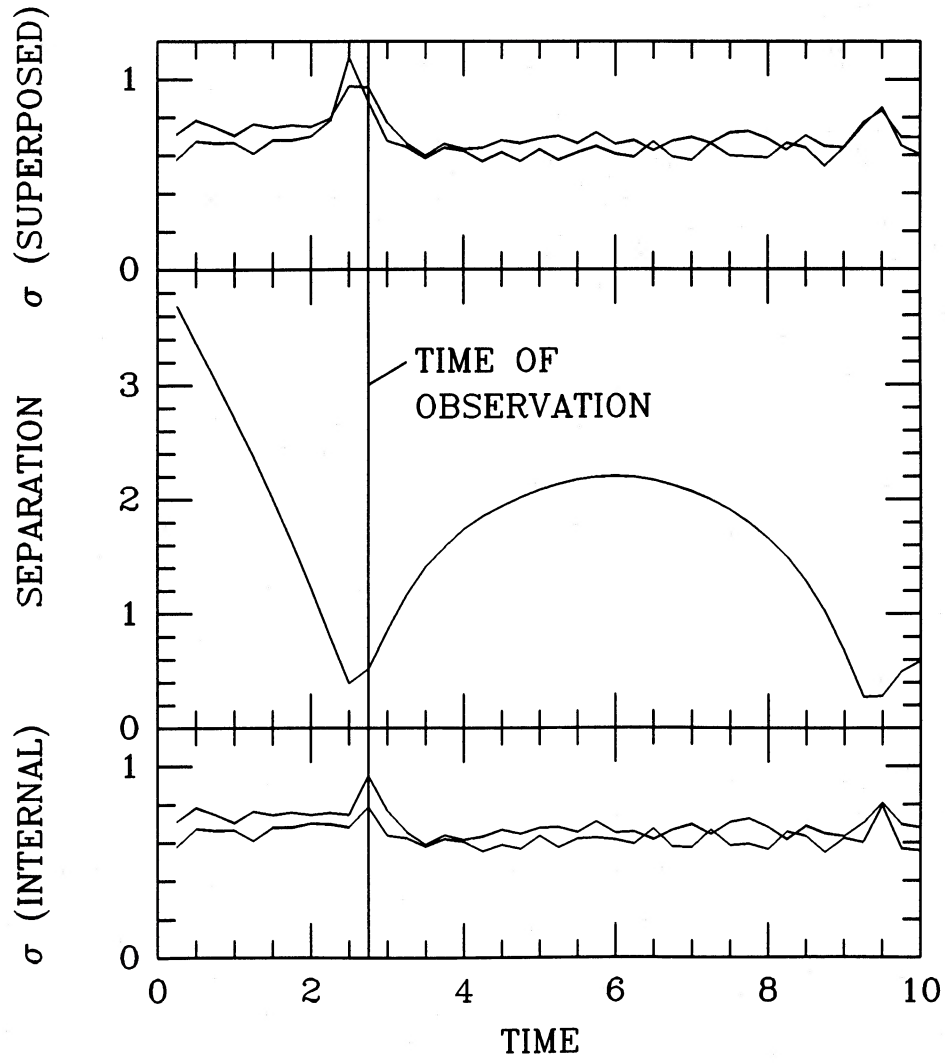

FIG. 11.—Time variations of several parameters for the N-body simulation described in § VI*a*. Model units are converted to physical units in § VIII. The middle box shows the time dependence of the binary separation, with pericenter passage at $T = 2.5$; the initially unbound binary merges at $T = 12$. The vertical line at $T = 2.75$ identifies the time of observation as deduced from the best match of the simulation to the observations of NGC 4782/4783. The upper panel presents two curves showing the time variations of the "observed" stellar velocity dispersions in the centers of the two model galaxies, where the more massive galaxy (NGC 4782) is represented by the upper curve. The peaks at $T = 2.5$ correspond to the time of maximum superposition (i.e., closest approach). The lower panel presents the time variations of the internal, uncontaminated stellar dispersions at the centers of the model galaxies (i.e., the contribution from the superposed stars in the other galaxy is suppressed). The tidal shocks (i.e., dispersion maxima) at $T = 2.75$ occurred coincidentally at the deduced time of observation.

Smith (1980) who argue that the sudden compression and expansion of colliding galaxies at closest approach demand a physically consistent method of numerical simulation.

Figure 11 shows the time variation of physical quantities in the N-body simulation. The middle box presents the binary separation. At $T = 0$, the separation is 4.0 units, with the galaxies approaching on a hyperbolic trajectory (orbital eccentricity = 1.03). During the close encounter the pair becomes bound through the action of tidal friction. Note that the first pericenter passage occurs at $T = 2.5$, and the time of observation, as determined from the best match to the data, is $T = 2.75$. The latter is identified by the vertical line drawn through all the boxes of Figure 11. Ultimately the pair merges at $T = 12$ (not shown here; see § VIII for the conversion from model to physical units).

The upper box in Figure 11 shows the time variation of the "observed" (i.e., integrated along the line of sight) central stellar velocity dispersions for the two model galaxies; the higher curve is for the more massive galaxy. These values were measured at the centers of the model galaxies using a small aperture (with a diameter roughly equal to the galaxy effective radius). No points are plotted until $T = 0.25$ (roughly one dynamical time), since the initial states of the model galaxies were not perfectly phase-mixed, and it would be irrelevant to compare the velocity dispersions before that time with the later values. The plotted dispersions show a dramatic increase at the time of pericenter passage ($T = 2.5$) when the two galaxies strongly overlap. Two factors contribute to these sudden enhancements in the dispersions: (1) contamination of "starlight" in one galaxy by stars from the other galaxy, leading to the mixture of two line-of-sight velocity distributions whose means differ by many hundred km s^{-1}; and (2) a tidal shock in each galaxy, where the sudden increase in the gravitational acceleration that each star experiences when the two galaxies strongly interpenetrate has physically increased the individual stellar velocities, and hence their overall dispersions.

The tidal shock can be visualized by measuring the line-of-sight velocity dispersions at the centers of the two galaxies using only the stars belonging to that galaxy, removing the contaminating stars from the other galaxy that appear within the aperture. This is a simple procedure when working with numerical simulations, but an obviously impossible task in the laboratory we call "the real universe." The corresponding curves (lower box in Fig. 11) thus show the purely internal variations of the stellar velocities in the core of each galaxy. We were gratified to find that there was indeed a tidal shock (i.e., stellar dynamical heating) when the two galaxies came closest together, and that the peak occurred just after pericenter passage, at the precise moment when our models best fit the full complement of observations for this pair of galaxies (i.e., at time $T = 2.75$). This was a purely fortuitous coincidence, as our orbit-search procedure was not aimed at finding a tidal shock. In retrospect, we believe that the tidal shock was required in the models in order to best match the observed dispersions in the two galaxies.

We can conclusively state (1) that the large central projected velocity dispersions measured in NGC 4782 and 4783 are a direct consequence of the strongly penetrating close encounter that the galaxies are experiencing, (2) that there is currently some superposition of starlight from one galaxy against the center of the other, (3) that, due to the tidal shock, the galaxies are not in dynamical equilibrium, and (4) that the pair is just beyond its point of closest approach. That there would be a phase lag between the time of pericenter passage and the time when the stellar velocity dispersion reaches it peak was predicted by Miller and Smith (1980). This lag is a result of the finite time needed for the increased gravitational forces, imposed by the overlapping galaxy mass distributions, to accelerate the stars to high velocities.

b) Tidal Distortions, Stripping, and Friction

It is interesting to examine the physical origin for the distortions seen in these galaxies. Paper II carried out such an analysis in the context of the $R_{\rm peri}$-$V_{\rm peri}$ orbit parameter space. Here we use a slightly different representation, shown in Figure 7. Figure 12 presents a schematic of this initial orbit parameter space. When the initial orbit has a low relative velocity and a small impact parameter (region A), the collision between the two galaxies will be nearly head-on. Assuming a nearly isotropic stellar velocity distribution $f(v)$ in the galaxies, the tidal distortions will be cylindrically symmetric with respect to the line of encounter: there will be very little asymmetry in the distortion in directions transverse to the orbital motion, even though there may be severe distortion along the line connecting the galaxy centers. Note that this conclusion changes if either of the galaxies is strongly rotating; in that case, there is a preferred plane of motion for the perturbed stars, leading to the formation of the familiar tidal tails and bridges.

At high initial relative velocity and large impact parameter (region B of Fig. 12), the tidal force will be very small and of short duration, producing only minor disturbances in the stellar mass distribution. This corresponds to the impulse approximation, where the form of the stellar velocity distribution is irrelevant. In the case where the initial relative velocity of the binary is low and the impact parameter is large (region C), the pair will fall together on a nearly linear trajectory at relatively low speed. The collision-induced distortions will be quite strong, but only a limited range of viewing angles would be available to match the observed small velocities, which would make it very difficult to match at the same time the compression angles observed in the images. Such collisions are just not energetic enough to account for the observations of NGC 4782/4783. In cases where the initial relative velocity is high and the impact parameter is small (region D), the distortions are not well developed at the time of observation due to the small impulse applied to the stars in a very rapid passage, and they have the wrong orientation with respect to the projected position vector. If one waits for the distortions to grow, the pair will be too far apart to match the observed separation and velocities, and the distortions will phase-mix within the galaxy.

In order to fully match the tidal distortions in NGC 4782/4783, the duration and the strength of the tides in our simulation must therefore be within a very restricted range of values. The duration of the tide is measured by $R_{\rm peri}/V_{\rm peri}$, and the tidal impulse by $(R_{\rm peri} \times V_{\rm peri})^{-1}$ (see Paper II). It is therefore no coincidence that the diagonal of near-solutions described in § IV*d* all have nearly identical values of $R_{\rm peri}$ and $V_{\rm peri}$ (see § IV*c*). Without dynamical friction, and hence with no orbital evolution, there would be a unique initial orbit that had the requisite pericenter speed and separation. That orbit is marked schematically by K in Figure 12 (for an energy-conserving, constant angular momentum pseudo-Keplerian trajectory). Because the orbits of interacting galaxies do decay, a range of initial orbits (region E) is permitted, where each orbit will lead to the proper tidal strength and duration.

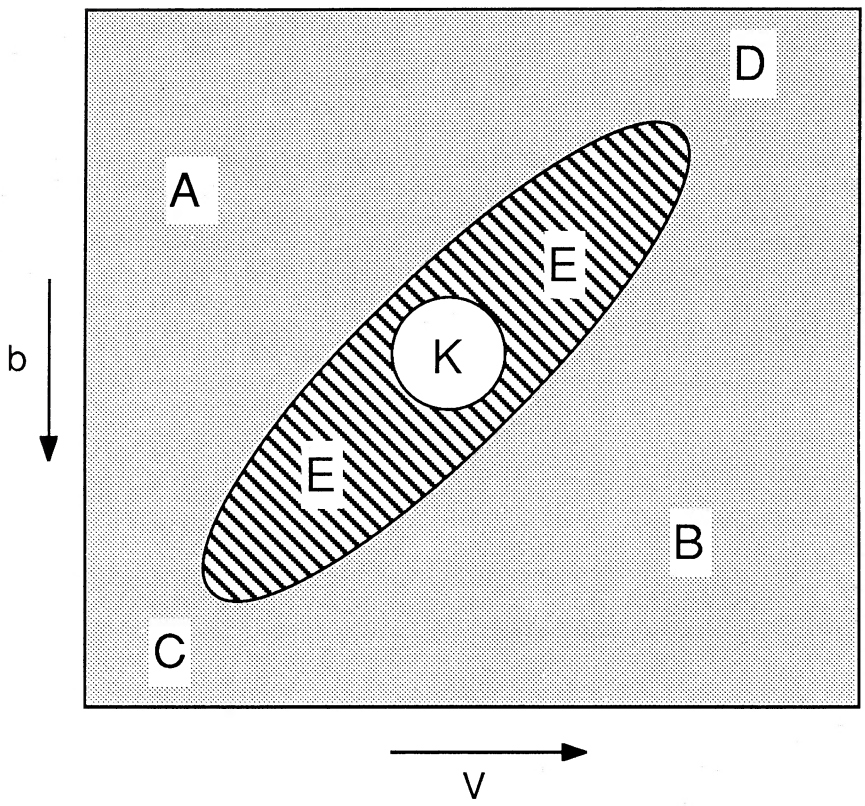

FIG. 12.—Schematic representation of the explored orbital parameter space that was presented in Fig. 7. Impact parameter increases downward, and initial speed increases to the right. Regions A, B, C and D are excluded for phyical reasons (see text). A point, labeled "K," corresponds, in the absence of tidal and dynamical friction, to the one ideal Keplerian orbital solution for NGC 4782/4783, whereas the extended region E presents the range of possible orbit solutions that correspond to similar pericenter speeds and pericenter separations as a result of friction and orbital evolution.

The observational parameters that have helped us locate a unique solution and that are most obviously affected by variations in the initial orbit parameters (i.e., by moving around in Fig. 12) are the compression angles β_i and the compression indices c_i for each galaxy. But why? The driving physical mechanism is a tidal coupling between resonant stellar orbits and the binary orbit (see Papers I and III). Prograde stars will experience a perturbation with a long time constant that remains more or less in phase with the orbit of the star, whereas retrograde stars will experience an oscillating perturbation that has a rapidly varying phase (see Borne and Hoessel 1985, and Paper III). It is therefore the prograde stars that are preferentially removing orbital energy and angular momentum from the perturbing galaxy. These are the stars that are being tidally stripped, and which are depicted in the asymmetric lobes of the surface brightness contour maps. As shown in Figure 10, the material that is being stripped does indeed trail behind the parent galaxy. Borne and Hoessel (1985) and Paper III argued that lobes such as these, as well as other dynamical signatures in interacting binaries, provide evidence for tidal friction in action. As a result of the energy loss during this and subsequent close passages, the two galaxies NGC 4782 and 4783 will merge into a single dynamical system. In our best-fit model this will occur 800 million years from now.

VII. DARK MATTER AND GROUP MEMBERSHIP

All of our simulations were run without massive halos. Even so, the ability to match the observed data with our models does not disqualify the massive halo hypothesis for elliptical galaxies (e.g., Forman, Jones, and Tucker 1985). At separations of order 10–20 kpc, where the luminous matter dominates the galactic potential, an extended halo is of almost no consequence. Because dark matter is not included, the simulations presented here only sample the mass on the scale of the luminous material.

De Souza and Quintana (1988) have shown that a group composed mostly of early-type galaxies surrounds the pair NGC 4782/4783, with a total of 20–25 members brighter than 16.5 mag. Radial velocities for 13 members yield a total virial mass of 3–7 $\times$ 10^{13} $M_\odot$, enough to make NGC 4782 and NGC 4783 bound to the group even before the binary collision, since the asymptotic velocity at large separation for our derived incoming binary orbit is 130 km s^{-1}. Because the group is not compact, the binary interaction is uncoupled from the group dynamics. Only one of the group members, NGC 4794, has luminosity comparable to the central pair, but that galaxy appears at a projected separation of 9′ from the pair, in a region far from the inbound trajectories of NGC 4782 and NGC 4783, and so it has not interacted with them in the recent past. The interaction between NGC 4782 and NGC 4783 is consequently a well-defined binary problem, and even though both NGC 4782 and NGC 4783 are bound to the group, the pair itself was unbound before the interaction, and is now a bound binary as a result of the collision. De Souza and Quintana have incorrectly criticized our model for this system, believing that we are saying that the NGC 4782/4783 pair was

initially not bound to anything. We emphasize that, since our models trace the mass in the general region of the luminous matter only, we are only proposing that the luminous parts of the two galaxies were initially unbound to one another. Our description of the NGC 4782/4783 pair is therefore not in conflict with the existence of the group, nor with the virial mass determination. In fact, the existence of the group nicely explains what otherwise would have been a very unlikely encounter in the field. Our dynamical study provides the mass on the size scale of the luminous matter, whereas the virial determination probes scales up to the size of the whole group. We believe that, on the small scale, our proposed orbital solution is entirely satisfactory. Our merger time estimate remains valid as well unless the highly eccentric binary orbit is perturbed in an encounter with another member of the group.

One result related to massive halos that is derivable from our best-fit model solution is the near-equality of M/L for the two galaxies. This can be seen as follows. If the two galaxies had very different M/L, then the relationship between $f_{\rm int}$ and $f_{\rm tot}$ for the mass distribution would differ from the corresponding relationship that we actually observe for the luminosity distribution. For example, in a hypothetical series of models where the mass of, say, galaxy 1 increases relative to that of galaxy 2, the mass projected inside the critical isophote for galaxy 1 would increase faster than its mass since both the tidal distension and tidal stripping of galaxy 2 would increase with the mass of galaxy 1, leading to an increasingly stronger contamination of the light in galaxy 1 by distended and stripped luminous material from galaxy 2. The values for $f_{\rm tot}$ and $f_{\rm int}$ would then diverge, rendering a mismatch with the actually observed near equality of those two luminosity ratios (§ II*a*). In other words, we may find a set of viewing angles for which the separation indices χ_1 and χ_2 have the correct values, but for which the ratio $f_{\rm tot}$ in the model is inconsistent with the corresponding $(L_2/L_1)_{\rm tot}$ value measured photometrically. Consequently, the M/L ratios within NGC 4782 and NGC 4783 must be very similar, with the light accurately tracing the mass.

VIII. SUMMARY

We have determined the masses and orbital parameters for the galaxies in the strongly interacting binary NGC 4782/4783 by finding a numerical simulation of the collision that accurately represents all of the observed properties of the system. With this simulation, we have completely determined the three-dimensional orientation and the dynamical state of the binary. The large relative velocity observed for the pair is the consequence of a high-speed encounter and is not an indicator of large galaxian masses. Large stellar velocity dispersions provide evidence for a tidal shock and are likewise not indicative of a large amount of mass.

Some of the physical parameters that define our solution for the pair are (for $H_0 = 60$ km s^{-1} Mpc^{-1}): log $M_{\rm tot}/M_\odot = 12.14$, $(M/L_{\rm B})_{\rm tot} = 10\ M_\odot/L_\odot$, mass of NGC 4782 $= 8.1 \times 10^{11}\ M_\odot$, pair mass ratio = 0.7, true relative velocity in plane of orbit = 690 km s^{-1} (649 km s^{-1} is the line-of-sight relative velocity), asymptotic velocity at large separation = 130 km s^{-1}, true separation in plane of orbit = 20.0 kpc (14.2 kpc is the observed projected separation), time since pericenter passage $\approx$ 25 million years, and time until merger (i.e., pair coalescence) = 800 million years. To translate from the model units used in this paper to their physical values, note that 1 velocity unit equals 346 km s^{-1}, that 1 distance unit equals 29 kpc, and that one time unit equals 82 million years. Our model makes specific predictions about the internal variations of velocity dispersion and mean velocity across the face of the galaxies. Multiposition dynamical data will be required either to validate or to repudiate our solution.

The existence of a group of galaxies around NGC 4782 and 4783 does not invalidate our treatment, because the binary interaction is uncoupled from the group dynamics. Our mass measurement invalidates the apparent causal link between the large internal dispersions and the supermassive nature of NGC 4782 and 4783 derived from the group dynamics by de Souza and Quintana (1988). The discrepancy between our mass estimate and theirs suggests that most of the dark material is located at large radii.

The galaxies are now just past pericenter passage, and there is evidence for a strong tidal shock, confirming predictions about the existence and phase lag of such shocks from numerical experiments by Miller and Smith (1980). The shock will lead to the loss of a large amount of mass from each galaxy. In fact, tidal truncation is already evident in the radial luminosity distribution for each galaxy (Figs. 5*a* and 5*b*). Large velocity dispersions (from the shock) and strong distortions in the luminous matter distribution provide evidence for tidal stripping and tidal transfer of orbital energy and angular momentum into individual stars. We are consequently witnessing tidal friction in action. This friction has led to the capture of the galaxies into a bound orbit and will ultimately lead to their coalescence into a single dynamical system.

We have demonstrated the value of a particularly rapid numerical integration scheme in the study of interacting galaxies. A large number of different orbits can be tested for a possible match to a set of observations. When a simulation comes close to matching the data, one can adjust the parameters as far as one desires, at little expense, until a detailed match is found. Enough information is available and quantifiable in the distorted luminosity distributions of the real system to uniquely specify a significant number of model input parameters. An N-body simulation for one of our better matching models substantiated the accuracy of the orbit solution and tidal distortions derived from the much faster MTBA simulation. In fact, two of us independently found the same solution, thereby confirming the robustness of our search method and of the numerical algorithm.

One of us (K. B.) was supported by a Carnegie Fellowship during the initial stages of this work. We thank the Space Telescope Science Institute for supporting another one of us (M. B.) during part of this. At the University of Wisconsin, partial support was provided by a subcontract to NASA contract NAS7-918. We are grateful to the director of the Kitt Peak National Observatory for the allocation of telescope time to this project.

REFERENCES

Arp, H. C. 1966, *Ap. J. Suppl.*, **14**, 1.
Arp, H. C., and Madore, B. F. 1987, *A Catalogue of Southern Peculiar Galaxies and Associations* (Cambridge: Cambridge University Press).
Baily, M. E., and MacDonald, J. 1981, *M.N.R.A.S.*, **194**, 195.
Blandford, R. D., and Icke, V. 1978, *M.N.R.A.S.*, **185**, 527.
Borne, K. D. 1984, *Ap. J.*, **287**, 503. (Paper I).

Borne, K. D. 1988*a*, *Ap. J.*, **330**, 38 (Paper II).
———. 1988*b*, *Ap. J.*, **330**, 61 (Paper IV).
Borne, K. D., and Hoessel, J. G. 1985, *Bull. AAS*, **17**, 601.
———. 1988, *Ap. J.*, **330**, 51 (Paper III).
Borne, K. D., and Richstone, D. O. 1982, *Bull. AAS*, **14**, 972.
——— 1988, in preparation.
Burbidge, E. M., Burbidge, G. R., and Crampin, D. J. 1964, *Ap. J.*, **140**, 1462.
Cowie, L. L., and Hu, E. M. 1986, *Ap. J. (Letters)*, **305**, L39.
Davies, R. L., Efstathiou, G., Fall, S. M., Illingworth, G., and Schechter, P. L. 1983, *Ap. J.*, **266**, 41.
Davies, R. L., and Illingworth, G. 1983, *Ap. J.*, **266**, 516.
de Souza, R. E., and Quintana, H. 1988, *A.J.*, submitted.
de Vaucouleurs, G. 1958, *A.J.*, **63**, 253.
de Vaucouleurs, G., de Vaucouleurs, A., and Corwin, H. G. 1976, *Second Reference Catalogue of Bright Galaxies* (Austin: University of Texas Press).
Faber, S. M., and Jackson, R. E. 1976, *Ap. J.*, **204**, 668.
Fall, S. M. 1981, in *The Structure and Evolution of Normal Galaxies*, ed. S. M. Fall and D. Lynden-Bell (Cambridge: Cambridge University Press).
Forman, W., Jones, C., and Tucker, W. 1985, *Ap. J.*, **293**, 102.
Greenstein, J. L. 1961, *Ap. J.*, **133**, 335.
———. 1962, *Ap. J.*, **135**, 679.
Hausmann, M. A., and Ostriker, J. P. 1978, *Ap. J.*, **224**, 320.
Hernquist, L., and Quinn, P. J. 1987, *Ap. J.*, **312**, 1.
Hoessel, J. G. 1980, *Ap. J.*, **241**, 493.
Hoessel, J. G., Borne, K. D., and Schneider, D. P. 1985, *Ap. J.*, **293**, 94.
Hoessel, J. G., and Schneider, D. P. 1985, *A.J.*, **90**, 1648.
Holmberg, E. 1937, *Lund Ann.*, **6**.
Jenner, D. C. 1974, *Ap. J.*, **191**, 55.
Karachentsev, I. D. 1972, *Comm. Special Ap. Obs. USSR*, **7**, 3.
Kormendy, J. 1985, *Ap. J.*, **295**, 73.
Kriss, G. A., Malumuth, E. M., and Borne, K. D. 1988, in preparation.
Landolt, A. U. 1973, *A.J.*, **78**, 959.
Malin, D. F., and Carter, D. 1983, *Ap. J.*, **274**, 534.
Michard, R. 1980, *Astr. Ap.*, **91**, 122.
Miller, R. H., and Smith, B. F. 1980, *Ap. J.*, **235**, 421.
Page, T. L. 1952, *Ap. J.*, **116**, 63.
Poveda, A. 1958, *Bol. Obs. Tonantzintla y Tacubaya*, **17**, 3.
Quinn, P. J. 1982, Ph.D. thesis, Australian National University, Canberra.
———. 1984, *Ap. J.*, **279**, 596.
Sandage, A., and Tammann, G. A. 1975, *Ap. J.*, **196**, 313.
Schweizer, F. 1982, *Ap. J.*, **252**, 455.
Stocke, J. T. 1978, *A.J.*, **83**, 348.
Terlevich, R., Davies, R. L., Faber, S. M., and Burstein, D. 1981, *M.N.R.A.S.*, **196**, 381.
Tonry, J. 1983, *Ap. J.*, **266**, 58.
———. 1985, *A.J.*, **90**, 2431.
Tonry, J., and Davis, M. 1981, *Ap. J.*, **246**, 666.
Toomre, A. 1977, in *The Evolution of Galaxies and Stellar Populations*, ed. B. M. Tinsley and R. B. Larson (New Haven: Yale University Observatory), p. 401.
Toomre, A., and Toomre, J. 1972, *Ap. J.*, **178**, 623.
White, S. D. M. 1982, in *Morphology and Dynamics of Galaxies*, Saas-Fee course **12** (ed. L. Martinet and M. Mayor), p. 289.
———. 1983, *Ap. J.*, **274**, 53.

MARC BALCELLS and JOHN G. HOESSEL: Department of Astronomy, University of Wisconsin, 475 N. Charter St., Madison, WI 53706

KIRK D. BORNE: Space Telescope Science Institute, 3700 San Martin Dr., Homewood Campus, Baltimore, MD 21218